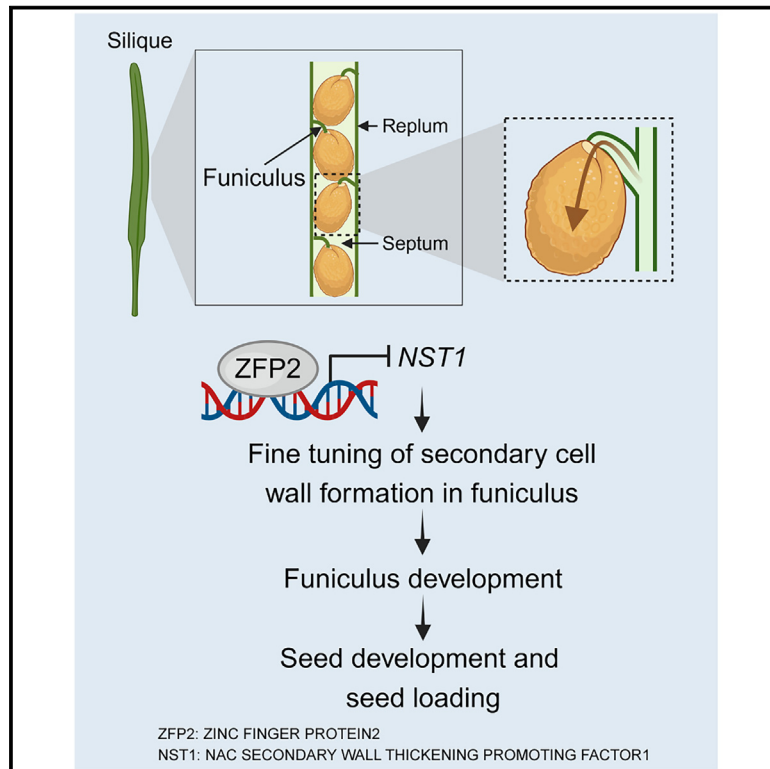


# Developmental Cell

## ZINC FINGER PROTEIN2 suppresses funiculus lignification to ensure seed loading efficiency in *Arabidopsis*

### Graphical abstract



### Authors

Pui Man Low, Que Kong, Leonard Blaschek, ..., Deyang Xu, Staffan Persson, Wei Ma

### Correspondence

staffan.persson@plen.ku.dk (S.P.),  
weima@ntu.edu.sg (W.M.)

### In brief

Low et al. identified a transcriptional regulator, ZFP2, which repressed ectopic secondary cell wall (SCW) formation in funiculi. The manuscript outlines a mechanism for how SCW biosynthesis is restricted to the vasculature of the funiculus to ensure appropriate seed loading in *Arabidopsis*.

### Highlights

- ZFP2 is important for *Arabidopsis* seed and silique development
- Loss of function of ZFP2 results in ectopic SCW formation in *Arabidopsis* funiculus
- ZFP2 acts as a transcriptional repressor of SCW formation
- ZFP2 directly targets SCW transcription factor NST1 to repress cortex cell lignification

Article

# ZINC FINGER PROTEIN2 suppresses funiculus lignification to ensure seed loading efficiency in *Arabidopsis*

Pui Man Low,<sup>1,5</sup> Que Kong,<sup>1,5</sup> Leonard Blaschek,<sup>2,5</sup> Zhiming Ma,<sup>1</sup> Peng Ken Lim,<sup>1</sup> Yuzhou Yang,<sup>1</sup> Trisha Quek,<sup>1</sup> Cuithbert J.R. Lim,<sup>1</sup> Sanjay K. Singh,<sup>3</sup> Christoph Crocoll,<sup>2</sup> Ellen Engquist,<sup>2</sup> Jakob S. Thorsen,<sup>2</sup> Sitakanta Pattanaik,<sup>3</sup> Wan Ting Tee,<sup>1</sup> Marek Mutwil,<sup>1</sup> Yansong Miao,<sup>1</sup> Ling Yuan,<sup>3</sup> Deyang Xu,<sup>2</sup> Staffan Persson,<sup>2,4,6,\*</sup> and Wei Ma<sup>1,6,7,\*</sup>

<sup>1</sup>School of Biological Sciences, Nanyang Technological University, Singapore 637551, Singapore

<sup>2</sup>Copenhagen Plant Science Center, Department of Plant and Environmental Sciences, University of Copenhagen, 1871 Frederiksberg, Denmark

<sup>3</sup>Department of Plant and Soil Sciences, Kentucky Tobacco Research and Development Center, University of Kentucky, Lexington, KY 40546, USA

<sup>4</sup>Joint International Research Laboratory of Metabolic & Developmental Sciences, State Key Laboratory of Hybrid Rice, School of Life Sciences and Biotechnology, Shanghai Jiao Tong University, Shanghai 200240, China

<sup>5</sup>These authors contributed equally

<sup>6</sup>Senior author

<sup>7</sup>Lead contact

\*Correspondence: [staffan.persson@plen.ku.dk](mailto:staffan.persson@plen.ku.dk) (S.P.), [weima@ntu.edu.sg](mailto:weima@ntu.edu.sg) (W.M.)

<https://doi.org/10.1016/j.devcel.2025.01.021>

## SUMMARY

The plant funiculus anchors the developing seed to the placenta within the inner dorsal pod strands of the silique wall and directly transports nutrients to the seeds. The lignified vasculature critically supports nutrient transport through the funiculus. However, molecular mechanisms underlying lignified secondary cell wall (SCW) biosynthesis in the funiculus remain elusive. Here, we show that the transcription factor ZINC FINGER PROTEIN2 (ZFP2) represses SCW formation in the cortex cells that surround the vasculature. This function is essential for efficient nutrient loading into the seeds. Notably, ZFP2 directly acts on the SCW transcription factor *NAC SECONDARY WALL THICKENING PROMOTING FACTOR1 (NST1)* to repress cortex cell lignification, providing a mechanism of how SCW biosynthesis is restricted to the vasculature of the funiculus to ensure proper seed loading in *Arabidopsis*.

## INTRODUCTION

Seeds are sophisticated structures that allowed seed plants to dominate terrestrial environments and serve as essential cornerstones of our global food supply.<sup>1</sup> Seed germination and subsequent seedling establishment require efficient mobilization of storage reserves to the seeds until the seedlings may support growth through photosynthesis.<sup>2,3</sup> Sufficient loading of the reserves poses significant challenges for plants but is a key driver of agronomic traits. Hence, plant breeders have invested considerable efforts in enhancing seed loading efficiency,<sup>3–5</sup> and several aspects of seed anatomy and physiology have been extensively investigated. These studies have clarified that the storage reserves typically constitute carbohydrates, oils, and proteins that predominantly are synthesized during the seed-filling phase.<sup>5–8</sup> The developing seeds rely on imported molecules, including sucrose, amino acids, and defense compounds (e.g., glucosinolates), to build the reserves and to fuel growth, particularly during maturation, and to protect plants after germination.<sup>9</sup> These molecules or

their precursors are transported from the maternal plant through the vascular tissues within the funiculus, ultimately reaching the seed coat, which distributes them to various seed compartments.<sup>3,10–12</sup> This sophisticated network of transportation underscores the critical role of the funiculus in seed development.

The funiculus serves as a critical anchor, connecting the developing seed to the placenta within the inner dorsal pod strands of the silique wall, and acts as the sole pathway between the silique septum and the seed for nutrient transport during seed development.<sup>3,12–14</sup> The funiculus is therefore considered an integral component of the plant vasculature.<sup>9</sup> A recent study showed that the funiculi in *Arabidopsis* are a major source of seed-bound glucosinolates,<sup>9</sup> which are primary defense compounds, in addition to their role in nutrient and photoassimilate transport. In *Arabidopsis*, glucosinolates encompass mainly tryptophan-derived indole glucosinolates and methionine-derived aliphatic glucosinolates, which are further divided into short-chained aliphatic glucosinolates (with three to five methylene groups, C3–C5) and long-chained aliphatic glucosinolates (with six to eight

methylene groups, C6–C8). Structural alterations to the funiculus occur in concert with seed development and are essential for the seed to grow.<sup>3,10,12–14</sup> During the transition from the ovule to the globular stage of seed development, the vascular strand, particularly the phloem, undergoes significant expansion by increasing the number of vascular cells, thereby enhancing metabolite transport to the seed.<sup>14</sup>

Plant cells are encased by cell walls, with expanding cells typically surrounded by thin primary walls that are composed of cellulose, hemicelluloses, and pectins.<sup>15–18</sup> The deposition of secondary cell walls (SCWs) in specialized cells such as the vascular tracheary elements occurs in concert with the cessation of cell expansion in certain cell types. SCWs are then formed inside of the primary walls and support mechanical strength, long-distance water and nutrient transport, resistance to biotic stress, fruit dehiscence, and pollen release.<sup>15,19–22</sup> SCWs primarily consist of cellulose, lignin, and hemicelluloses<sup>15,20,21,23</sup> with a corresponding set of biosynthetic genes with highly controlled expression patterns. These genes are controlled by a hierarchical network of transcriptional regulators.<sup>16,21,22,24</sup> Positioned at the top of this network are a group of closely related NAC-domain transcription factors (TFs). These SCW-associated NACs control an array of downstream TFs, notably MYB TFs, which subsequently control the expression of the SCW biosynthetic genes.<sup>16,20,22</sup> While much of this transcriptional framework is well characterized, regulatory aspects of the initiation and control of the upstream NAC regulators, also referred to as SCW master regulators, remain incomplete.

Zinc finger protein TFs are pivotal regulators, governing various cellular functions, such as transcription, translation, apoptosis, and protein-protein interactions.<sup>25,26</sup> Classified by the arrangement of histidine and cysteine residues, vital for the binding of zinc ions within the finger's secondary structure, zinc finger proteins fall into different groups, including C2HC, C2C2, C2H2, C2HCC2C2, and C2C2C2C2.<sup>26,27</sup> The *Arabidopsis* genome encodes 176 C2H2-type zinc finger proteins, among which 33 members are conserved across many eukaryotes, while the remaining 143 members appear to be specific to the plant kingdom.<sup>27</sup> C2H2 zinc finger proteins control a myriad of biological processes in plants, such as trichome growth and development,<sup>28–31</sup> shoot and flower development,<sup>31–37</sup> root hair development,<sup>38,39</sup> stress responses,<sup>39–42</sup> and hormone signal transduction pathways.<sup>29,30,32,37,39,43,44</sup> Here, we show that ZINC FINGER PROTEIN2 (*ZFP2*) represses SCW production in the funiculus by directly acting on the SCW master regulator *NAC SECONDARY WALL THICKENING PROMOTING FACTOR1* (*NST1*). This suppression precisely controls SCW synthesis in the funiculus to maintain effective seed loading.

## RESULTS

### *ZFP2* is necessary for seed and silique development in *Arabidopsis*

To explore possible regulators of seed development, we screened transfer DNA (T-DNA) lines of TFs that are expressed in the siliques based on publicly available microarray and RNA sequencing (RNA-seq) experiments.<sup>45–47</sup> Interestingly, we found that three independent T-DNA lines (*zfp2-1*, *zfp2-2*, and *zfp2-3*; Figures 1A and 1B), corresponding to the C2H2-type *ZFP2*, dis-

played altered silique shape and reduced seed size (Figures 1C and 1D). We verified the absence of *ZFP2* transcript in the three lines by reverse transcription PCR (RT-PCR) (Figure 1B). The *zfp2* mutants also displayed shorter siliques (Figure 1E), reduced seed weight (Figure 1F), as well as decreased seed area, perimeter, length, and width compared with wild type (WT) (Figure 1G). However, the seed number per silique between WT and *zfp2*s remained the same (Figure S1A).

To assess the seed content, we next analyzed various seed traits of *zfp2*. As shown in Figures 1H and S1B, seed oil accumulation from 11 to 19 days after pollination (DAP) was reduced in *zfp2-2* developing seeds compared with WT. Notably, the seed-bound long-chained aliphatic glucosinolate levels in mature seeds were reduced by 50% in *zfp2-1* and by more than 70% in *zfp2-2* and *zfp2-3* (Figure 1I), while the levels of the other seed-bound glucosinolates were not affected. Glucosinolate content and profile in the rest of the silique (i.e., silique walls, replum, septum, and funiculi) were not affected in *zfp2* mutants (Figure S1C). These data suggest a role of *ZFP2* in loading seed-bound metabolites and in the development of plant fruits and seeds.

### *ZFP2* is highly expressed in the non-seed tissues of *Arabidopsis* siliques

To outline a detailed map of the *ZFP2* expression, we first carried out quantitative real-time PCR (qRT-PCR) across various *Arabidopsis* tissues. While *ZFP2* was modestly expressed in stems and flowers, the highest expression was in the siliques (Figure 2A). We further dissected temporal *ZFP2* expression in developing siliques and observed that *ZFP2* was predominantly expressed in silique valves, as well as non-seed tissue inside the siliques, compared with developing seeds (Figure 2B). We next generated reporter *Arabidopsis* lines expressing  $\beta$ -Glucuronidase (*GUS*) driven by the native *ZFP2* promoter (*proZFP2:GUS*) to further detail the expression profile of *ZFP2* in siliques. Histochemical staining indicated that *ZFP2* was expressed in valves during the silique development (Figure 2C), corroborating our qRT-PCR results (Figure 2B). In addition, *GUS* signal was evident in non-seed tissues inside the siliques, such as funiculus and replum (Figure 2D). These data were corroborated by expression data from the funiculus and other seed regions across seed development<sup>12</sup> (Figure S2A). *ZFP2* is thus highly expressed in non-seed tissues of developing siliques in *Arabidopsis*.

As a TF, *ZFP2* is expected to act in the nucleus. To corroborate this, we transiently expressed a *YFP-ZFP2* fusion construct in *Nicotiana benthamiana* leaves, followed by confocal microscopy imaging. Our results show that *YFP-ZFP2* was localized in the nucleus (Figure S2B). In addition, we transformed the *zfp2-2* mutant with a construct expressing *FLAG-ZFP2-YFP* driven by *proZFP2* (*proZFP2:FLAG-ZFP2-YFP*) and found that the transgene complemented the shape-altered phenotype of *zfp2-2* (Figure S2C). Confocal microscopy showed the presence of *FLAG-ZFP2-YFP* in the nucleus of funiculus cells (Figure S2B).

### Loss of function of *ZFP2* leads to ectopic, fiber-like SCW formation in funiculi

The disrupted accumulation of long-chained glucosinolates in *zfp2* mutants next led us to the funiculus, which functions as a cell factory for the synthesis of seed-bound glucosinolates.<sup>9,48</sup>

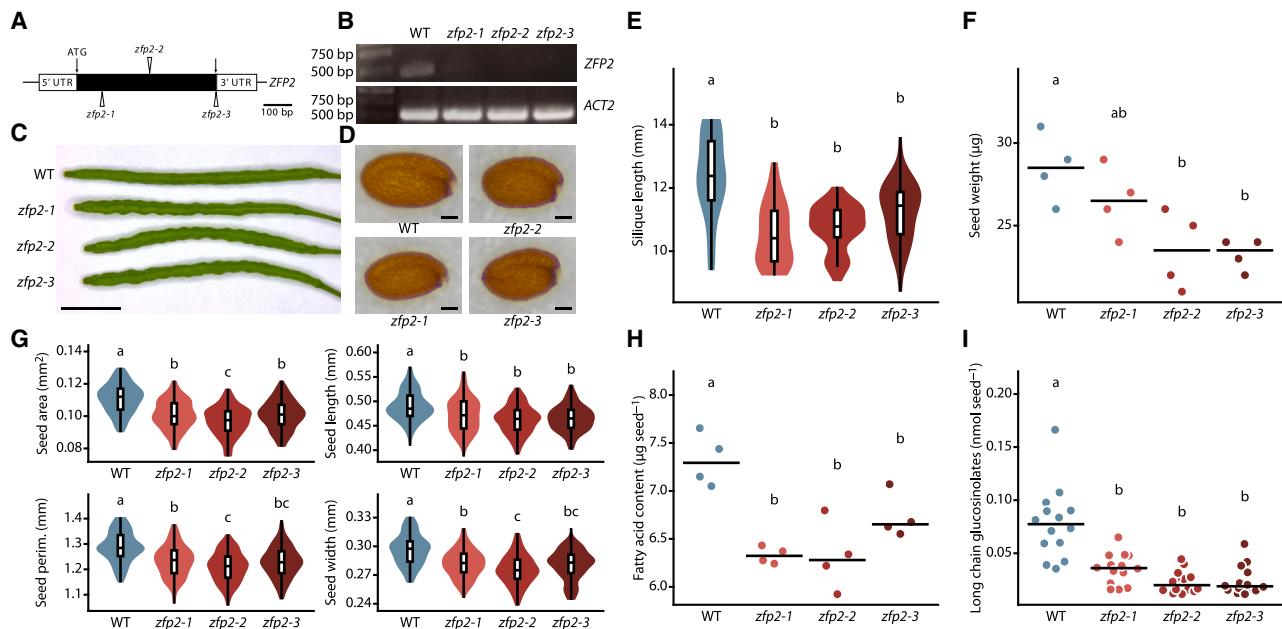


**Figure 1. Analyses of silique and seed phenotypes of WT and *ZFP2* loss of function mutants**

(A) Schematic diagram of T-DNA insertions in the *zfp2* mutants.  
 (B) *ZFP2* transcript accumulation in the three *zfp2* mutants was analyzed by reverse transcription PCR (RT-PCR). *ACT2* (*ACT2*) was used as a control.  
 (C) Appearance of siliques of WT and *zfp2* mutants at 7 DAP. Scale bar indicates 3 mm.  
 (D) Appearance of WT and *zfp2*s seeds. Scale bar indicates 100  $\mu$ m.  
 (E) Silique length of WT and *zfp2* mutants at 7 DAP.  $n = 28$ –33 siliques.  
 (F) Seed weight of WT and *zfp2* mutants was measured using 100 seeds per plant.  $n = 4$ .  
 (G) Seed area, perimeter, length, and width of WT and *zfp2* mutants.  $n = 100$ –120 seeds.  
 (H) Total seed oil content in WT and *zfp2* mutants.  $n = 4$ .  
 (I) Aliphatic long-chain glucosinolate content per seed, measured from pools of 10 seeds from one silique per plant.  $n = 14$  plants. Horizontal lines indicate the group median. Different letters indicate statistically significant differences between genotypes according to a one-way ANOVA followed by a Tukey-HSD test ( $\alpha = 0.05$ ).

As *ZFP2* was highly expressed in the funiculus, we next investigated whether *ZFP2* contributes to the development of the funiculus by examining phenotypical consequences of *ZFP2* mutations in funiculi. We first collected siliques at the late stage 17,<sup>49</sup> 11–12 DAP. At this stage, silique differentiation and elongation are completed, and seed loading is ongoing. In WT funiculi, we observed lignified SCWs only in xylem tracheary elements in the center of the funiculus, and occasionally at the very tip of the funiculus, where the separation layer for seed dehiscence forms<sup>50</sup> (Figure 3A). By contrast, in *zfp2* mutants, we observed a centripetal spread of ectopic, lignified SCWs (eSCWs) in cortex cells, particularly in the first to third cell layer, along the whole length of the funiculus. Lignin accumulation in eSCWs was further confirmed using the Wiesner test, which specifically stains lignin coniferaldehyde residues (Figure S3A). These eSCWs were clearly differentiated from lignified primary cell walls, a common stress response, by the substantial accumulation of additional cellulose to form bona fide SCWs (Figure 3A). The eSCWs were deposited evenly, setting them apart from the annular or spiral patterning of xylem tracheary elements in funiculi. Their morphology was therefore more similar to fiber SCWs, which are not formed in WT funiculi at this growth stage (Figure 3A). The densities of the eSCWs were intermediate in *zfp2-1* but highest in *zfp2-2* and *zfp2-3* (Figure 3B), consistent

with observed decreases in seed weight and glucosinolate levels. These eSCWs completely surrounded the xylem, likely interfering with biosynthesis and transport of glucosinolates within funiculi (Figure 1). Additionally, the eSCWs also appeared to limit cortex cell elongation in *zfp2* funiculi (Figures 3C and 3D). The reduction in funiculus length, together with a likely reduction in flexibility, could perhaps explain why the seeds in *zfp2* siliques are not arranged into a flat lattice, potentially leading to the observed crinkly silique phenotype (Figure 1C). In contrast to the eSCW deposition in funiculus, we did not find evidence for differential lignin accumulation in stems nor changed lignification patterns in the silique valve and replum (Figure S3B).

### ***ZFP2* negatively controls the expression of SCW biosynthesis genes**

To gain insights into the potential downstream target genes of *ZFP2*, we analyzed the global expression profiles of *zfp2-2* siliques using RNA-seq. The global transcriptomes of WT and *zfp2-2* showed significant differences as indicated by principal-component analysis (PCA) (Figure S4A), with 324 genes being differentially expressed in *zfp2-2* compared with WT (Figure S4B). Among these, more than half (56.5%) were upregulated in *zfp2-2*. Gene Ontology (GO) enrichment analysis suggested that many of the upregulated genes were involved in

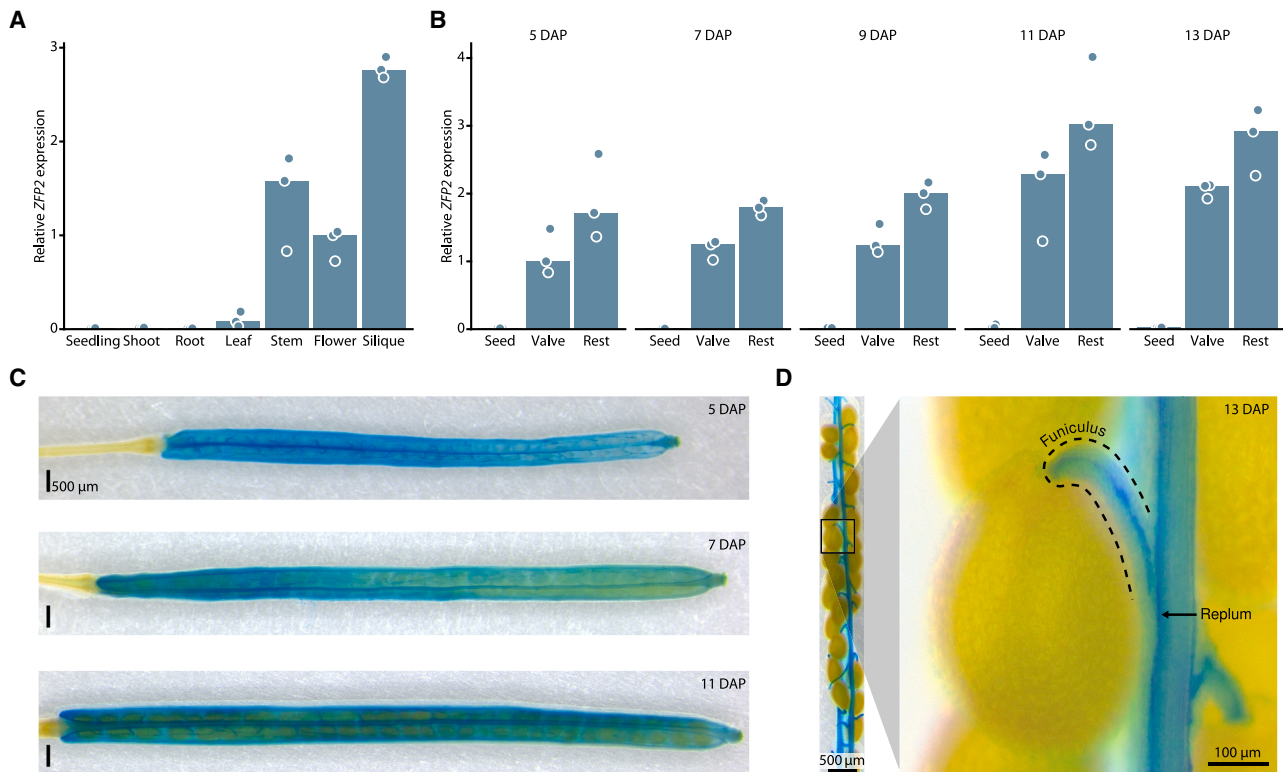


**Figure 2. Expression analysis of ZFP2 in Arabidopsis**

(A) ZFP2 transcript accumulation in different tissues of WT *Arabidopsis* was measured by quantitative real-time PCR (qRT-PCR).  $n = 3$ .  
 (B) ZFP2 transcripts in silique valves, seeds, and remaining tissues such as replum and funiculus (rest) in WT at 5, 7, 9, 11, and 13 days after pollination (DAP) were determined by qRT-PCR.  $n = 3$ . Bar height indicates the group median.  
 (C) GUS staining in siliques of a representative *proZFP2:GUS* transgenic line showing ZFP2 expression in valves of developing siliques at 5, 7, and 11 DAP.  
 (D) GUS staining in 13 DAP siliques of a representative *proZFP2:GUS* transgenic line after removal of valves, showing ZFP2 expression in replum and funiculus.

SCW biosynthesis (Figures S4B and S4C). Considering the fiber-like architecture of the eSCWs in the *zfp2* funiculi, the upregulation of the fiber-specific SCW transcriptional regulator *NST1* warranted special attention<sup>51–53</sup> (Figures S4B and S4C). We therefore examined the expression of *NST1* and several other SCW-related genes, namely *SND2*,<sup>54</sup> *MYB63*,<sup>55</sup> *LAC12*,<sup>56</sup> *LAC17*,<sup>56</sup> *IRX9*,<sup>57</sup> *IRX15*,<sup>58</sup> and *PRX52*,<sup>59</sup> using qRT-PCR and confirmed that they were indeed upregulated in *zfp2-2* compared with WT (Figure 4A). Similar results were obtained when we assessed the expression of SCW-related genes in siliques of *zfp2-1* (Figure S4D). We generated a *zfp2-2 nst1-1* double mutant and found that the increased expression of SCW-related genes in *zfp2-2* was significantly reduced in *zfp2-2 nst1-1* (Figure 4A). In addition, we examined the expression of several genes involved in fruit development and observed no significant difference between WT and *zfp2-2* (Figure S4E). These results suggest that ZFP2 plays a role in negatively regulating fiber-specific SCW gene expression in siliques.

### ZFP2 functions as a transcriptional repressor of SCW biosynthesis

To investigate whether ZFP2 controls fiber-specific SCW genes directly through *NST1*, we examined transactivation activity of ZFP2 using a dual-luciferase (LUC) assay in a *N. benthamiana*

transient expression system.<sup>60–62</sup> The ZFP2 was driven by the CaMV 35S promoter, and the LUC reporter gene was driven by the *NST1* promoter (*proNST1*) (Figure 4B). Our results showed a substantial reduction of LUC activity (Figure 4C), suggesting that ZFP2 repressed the activity of *proNST1* in plant cells. We also assessed ZFP2 effect on the promoter activities of two other SCW-related regulators, *SND2* and *MYB63* (*proSND2* and *proMYB63*), using the dual-LUC assay (Figure S5A). As shown in Figure S5B, ZFP2 significantly repressed the LUC activity for *SND2*, but not *MYB63*. To confirm that ZFP2 represses *NST1* *in planta*, we generated a *proNST1:GUS* reporter line (in WT background) and crossed it into the *zfp2-2* mutant background. Corroborating the above results, GUS signal in funiculi was drastically increased upon loss of ZFP2 (Figure S5C).

C2H2-type zinc finger proteins whose amino acid sequences are similar to ZFP2 can be divided into four subgroups, in which ZFP2 (subgroup I) is distinct from GLABROUS INFLORESCENCE STEMS (GIS) family members (subgroup IV) (Figure S5D). *In silico* analysis showed that ZFP2 harbored one typical C2H2-type zinc finger domain (containing the conserved QALGGH sequence<sup>26</sup>) and one low-complexity region (LCR) (Figure S5E). Moreover, we found that ZFP2 comprised three putative LxLxL-type ethylene-responsive element binding factor-associated amphiphilic repression (EAR) motifs (Figure 4B),

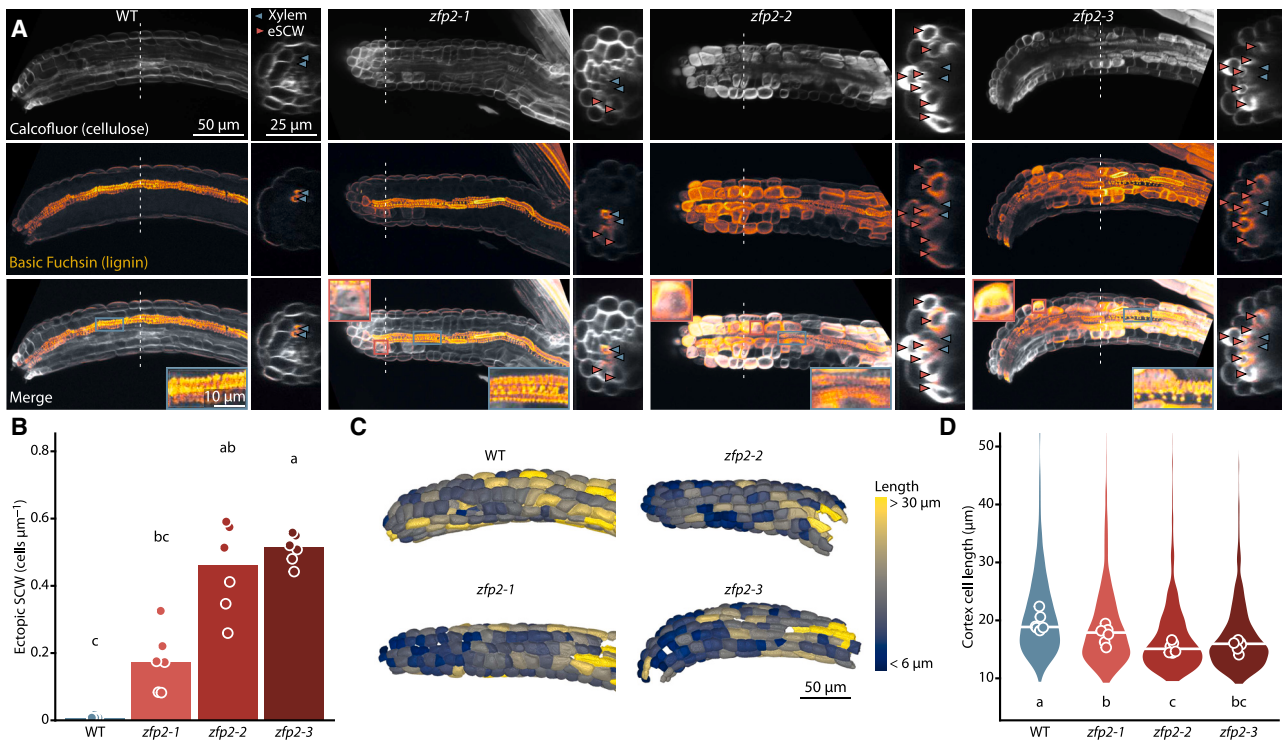


**Figure 3. Loss of ZFP2 leads to the ectopic formation of fiber-like lignified SCWs in funiculus**

(A) Cellulose and lignin distribution in 11–12 DAP funiculus, as visualized by Calcofluor white and basic fuchsin staining, respectively. Longitudinal optical XY cross-sections are projections of the 40 Z-slices surrounding the xylem (10 μm total). Dashed vertical lines indicate the position of the optical YZ-section shown alongside. Blue arrowheads indicate the position of xylem TEs, and red arrowheads indicate cells with eSCWs. Insets highlight the difference between the patterned SCWs of tracheary elements and the uniform thickenings of the fiber-like eSCWs in cortex cells.

(B) Density of eSCWs in 11–12 DAP funiculi ( $n = 6$  plants).

(C) Segmented funiculus cortex cells, colored by the diameter of their long axis.

(D) Cortex cell length in 11–12 DAP funiculi. Dots represent median cell length per replicate ( $n = 6$  plants). Violin plots show the distribution of individual cortex cells.

Bars and horizontal lines indicate the group median. Different letters indicate statistically significant differences between genotypes according to a Kruskal-Wallis test followed by Dunn's test, Holm-adjusted for multiple comparisons (B;  $\alpha = 0.05$ ), or a one-way ANOVA followed by a Tukey-HSD test (D;  $\alpha = 0.05$ ).

which potentially function as repression motifs.<sup>63–66</sup> Two EAR motifs (EAR1 and EAR2) are close to the N terminus, and the third EAR motif is in the C-terminal region of ZFP2 (Figure 4B). Deletion of the C-terminal EAR3 (ZFP2<sup>1–143</sup>) or mutation of EAR3 (L to A substitution; designated as ZFP2 mEAR3) resulted in reduced repression activity of ZFP2 (Figure 4C). Further deletion of the N-terminal EAR1 and EAR2 (ZFP2<sup>28–143</sup>) or mutation of EAR1 and EAR2 (designated as ZFP2 mEAR1-3) led to a further reduced repression activity of ZFP2 (Figure 4C). Hence, ZFP2 acts as a transcriptional repressor to control SCW biosynthetic genes through several EAR motifs.

### NST1 is a direct target gene of ZFP2

To assess how ZFP2 represses *NST1* expression, we next generated a chimeric ZFP2 protein (ZFP2-VP16) by fusing ZFP2 with the VP16 transcriptional activator domain.<sup>67</sup> Using this construct, we carried out dual-LUC transient expression assay to assess transactivation of ZFP2-VP16 on *proNST1* in *N. benthamiana* leaves (Figure S5F). As shown in Figure S5G, the ZFP2-VP16 was significantly less effective in suppressing *proNST1* as compared with ZFP2. Most plant zinc finger proteins

harbor a conserved QALGGH motif within their zinc finger helices, which is missing in animals and yeast.<sup>26</sup> This motif plays a vital role in DNA binding affinity in plants.<sup>26,68</sup> To test this for ZFP2, we mutated the ZFP2 (ZFP2<sup>L67H/G69V</sup>) by substituting leucine 67 (L67) and glycine 69 (G69) residues to histidine (H67) and valine (V69), respectively, and examined the effects on transactivation of *proNST1* (Figure S5H). Our result indicated that the ZFP2<sup>L67H/G69V</sup> was substantially less effective in repressing *proNST1* compared with the native form of ZFP2 (Figure S5I). These results imply that ZFP2 represses *NST1* expression via direct binding to *proNST1*.

To test whether ZFP2 is directly associated with the *NST1* locus, we next carried out chromatin immunoprecipitation (ChIP) assay using siliques of *proZFP2:FLAG-ZFP2-YFP/zfp2-2* plants. ChIP assay indicated that ZFP2 was strongly associated in a region upstream of the transcription start site (P6 fragment; Figures 5A and 5B), as well as the P2 fragment (Figures 5A and 5B), of the *NST1* promoter. Our ChIP result was further verified by electrophoretic mobility shift assay (EMSA). We designed four biotin-labeled DNA probes (probe P6-1 to P6-4) within P6 fragment that possessed ZFP2 binding elements (Figure 5C).

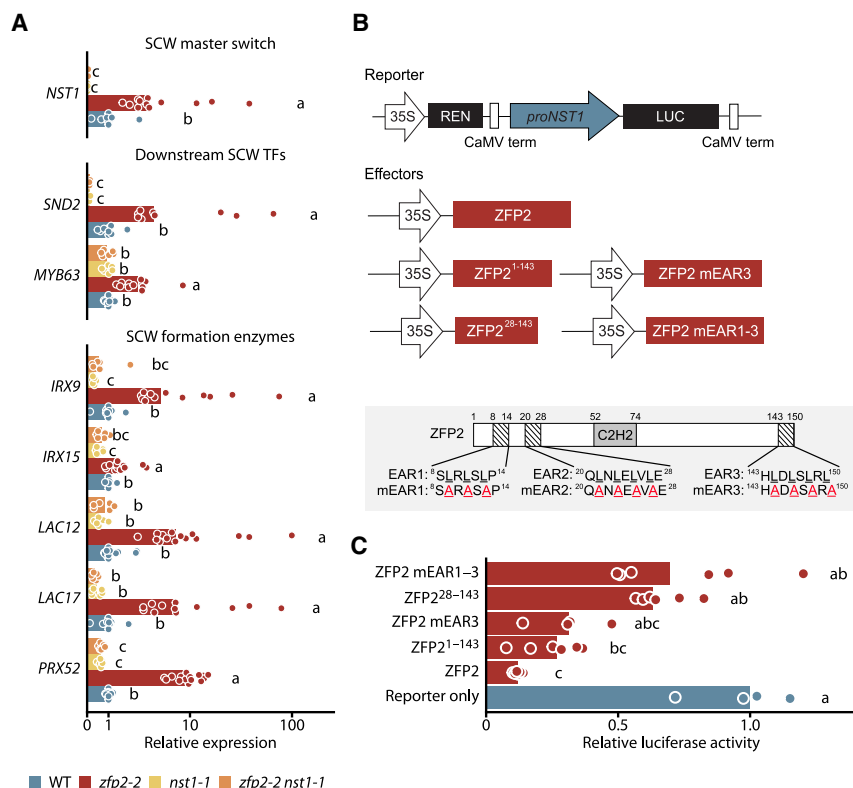


**Figure 4. ZFP2 functions as a transcriptional repressor**

(A) Expression levels of genes involved in SCW formation in siliques as analyzed by qRT-PCR.  $n = 6-12$  samples from 2 to 4 growth instances. Bars indicate the group median. Values are shown on a pseudo-log scale. Different letters indicate statistically significant differences between genotypes according to a one-way ANOVA followed by a Tukey-HSD test ( $\alpha = 0.05$ ).

(B) Schematic representation of the constructs and site-directed mutations used in the dual-luciferase (dual-LUC) assay in *N. benthamiana* leaves through transient expression.

(C) Transactivation of the LUC reporter by the different ZFP2 constructs in *N. benthamiana* leaves infiltrated either with the reporter alone or in combination with the effector. Renilla (REN) LUC was used as an internal control.  $n = 4-6$  replicates. Bars indicate the group median. Different letters indicate statistically significant differences between constructs according to a Kruskal-Wallis test followed by Dunn's test, Holm-adjusted for multiple comparisons ( $\alpha = 0.05$ ).

EMSA, using purified recombinant GST-His-ZFP2, indicated that ZFP2 protein could bind to the designed DNA probes (Figure 5C). As we progressively increased the unlabeled probe (10 $\times$  to 80 $\times$  of the cold probe) in the reaction mixture, we observed gradual disappearance of the labeling signal, indicating a high binding specificity of GST-His-ZFP2 to the labeled probes (Figure 5C). Collectively, our results show that *NST1* is a direct target of ZFP2.

## DISCUSSION

We outline that ZFP2 works as a key transcriptional regulator of SCW biosynthesis in funiculi and show that this function is required for the accumulation of seed-bound metabolites. ZFPs primarily control plant developmental processes and phytohormone signaling.<sup>26,28,29,31,32,36,38,43</sup> The involvement of ZFP2 in lignification, particularly as a previously uncharacterized transcriptional repressor in fruit tissues (such as funiculi), identifies a new research direction for the ZFP TF family.

ZFP2 is a C2H2-type zinc finger protein with three EAR motifs in its N and C terminus that confer the repression activity of ZFP2. Similarly, some other C2H2 zinc finger proteins also act as transcriptional repressors, such as KNUCKLES (KNU) and ZP1.<sup>37,38,69</sup> The repression activity in these TFs was primarily controlled via the interaction of their EAR motifs with TOPLESS (TPL), a transcriptional co-repressor that recruits histone deacetylase to change chromatin structure.<sup>66,70,71</sup> Additionally, a wealth of information indicates that these repressors function by interacting with the polycomb group (PcG) proteins. For

instance, SUPERMAN (SUP) represses the auxin biosynthesis genes by recruiting PcG complex, hence fine-tuning local auxin signaling to control floral meristem determinacy.<sup>37</sup> KNU recruits PcG to downregulate *WUSCHEL* (*WUS*), an essential gene in floral meristem determinacy.<sup>69</sup> Hence, it is plausible that also the EAR motifs of ZFP2 recruit histone deacetylases and/or PcG proteins to control transcriptional repression of SCW biosynthesis. Protein sequence alignment analysis of ZFP2 showed that EARs were conserved across ZFP2 from diverse plant species, including monocots and dicots (Figure S5E), suggesting a conserved molecular mechanism of gene regulation.

During the past two decades, a wealth of studies has demonstrated the gene regulatory network underlying SCW formation but primarily in vascular tissues of stems and roots.<sup>15,16,18</sup> *NST1* is a fiber-specific master regulator that initiates SCW formation by activating various SCW-related genes.<sup>15,16,18</sup> Nevertheless, there is limited information about transcriptional fine-tuning of *NST1* and its homologs, i.e., the VASCULAR-RELATED NAC-DOMAIN (VND) clade of NAC TFs. A previous study showed that *MYC2/MYC4* can activate *NST1* expression via direct binding to its promoter, thus promoting SCW thickening in stems.<sup>52</sup> Another study showed that *WRKY12* directly bound to the promoter of the *NST1*-homolog, *NST2*, and repressed its expression, leading to reduced SCW formation, again in *Arabidopsis* stems.<sup>72</sup> Interestingly, the *WRKY12* suppressed SCW formation in the cortex cells of the stems, similarly to what we observed for ZFP2 in the funiculus. The analogous functions of *WRKY12* and ZFP2 may assure that cortex cells of the stem and funiculus maintain their biological function. *WRKY12*, and potentially other suppressors, with partially redundant functions in stems and other tissues might also be the reason that stem lignification remained unchanged in *zfp2* plants. Indeed, in *zfp2* mutants, increased expression of genes

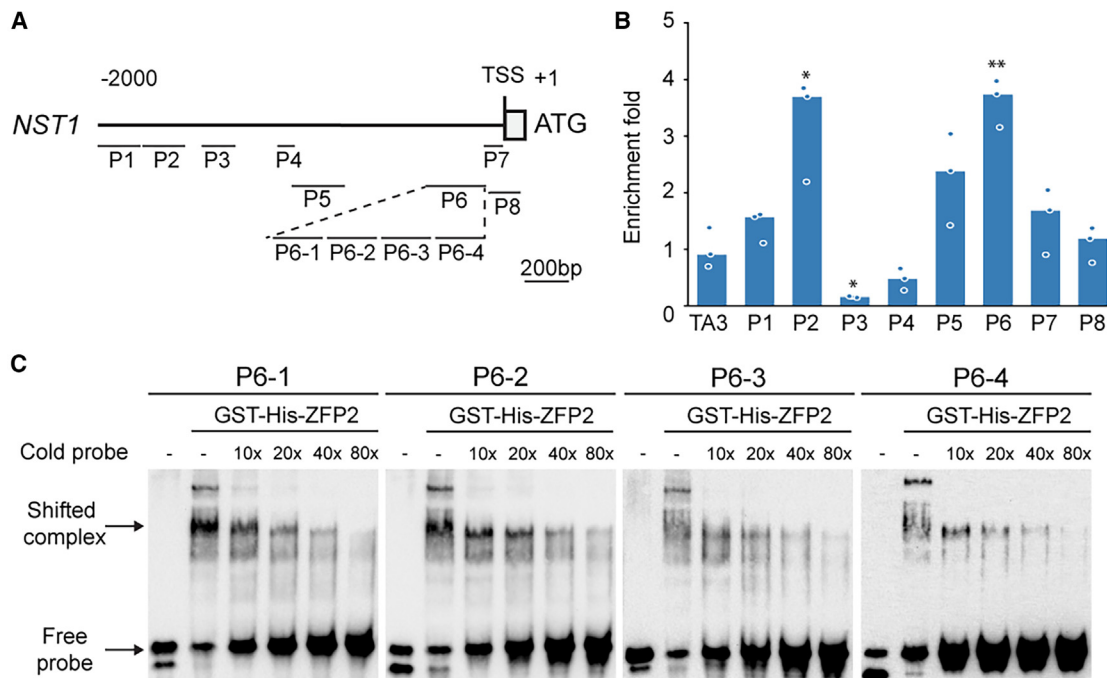


**Figure 5. *NST1* is a direct target of *ZFP2***

(A) Schematic diagram of *proNST1*. The first nucleotide of the translation start codon is assigned the +1 position. The 5' untranslated region is indicated by white box. P1 to P8 are shown as the regions used for chromatin immunoprecipitation (ChIP) assays.

(B) ChIP assay using siliques of *proZFP2:FLAG-ZFP2-YFP* in *zfp2-2*. TA3 retrotransposon (TA3) is used as the negative control locus, and the values of TA3 were calibrated to 1. The y axis shows relative enrichment fold by comparing with no antibody control. The bar height represents the group median of three technical replicates. The asterisks indicate significant differences between TA3 and different primer sets on *proNST1* (\*\* $p < 0.001$ , \*\* $p < 0.01$ , \* $p < 0.05$ , one-way ANOVA).

(C) Four DNA probes (covering the P6 region in the ChIP assay) were designed for electrophoretic mobility shift assay (EMSA) to investigate their interaction with purified GST-His-ZFP2. Binding of GST-His-ZFP2 to probe P6-1 to P6-4, respectively. Probes were labeled with biotin. Unlabeled probes (cold probes) were added with an increasing amount to compete with the biotin-labeled probes. The free probe and the shifted DNA-protein complex are indicated by arrowheads.

involved in SCW biosynthesis leads to eSCW specifically in funiculi, impeding the transport of metabolites to the seed. Notably, some other TFs that influence SCW deposition in funiculi, including HECATE3, SEEDSTICK, and ALCATRAZ, have been identified, but the transcriptional context of these TFs remains largely unexplored.<sup>50</sup> Our work therefore substantially advances the gene regulatory mechanism of SCWs and *NST1*, particularly in fruit tissues. How other factors, such as phytohormones and nutrients, contribute to the function of *ZFP2* in controlling SCW synthesis in funiculus will be the direction of future studies.

The funiculus, an umbilical cord-like structure, functions as a crucial anchor that links the developing seeds to the maternal plant.<sup>12,73</sup> Additionally, it is the sole pathway for direct transport of nutrients during seed development. The development of the funiculus is a dynamic process closely connected with seed growth.<sup>3,12</sup> The fact that the funiculus remains alive and intact throughout seed maturation in *Arabidopsis* suggests the contribution of all its tissue layers for seed development.<sup>12</sup> Indeed, recent discoveries indicate an important function of funiculus in the biosynthesis and subsequent transport of glucosinolates to the seeds.<sup>9,48</sup> We found reduced glucosinolate contents in *zfp2s*, furthering our understanding of nutrient routes from the funiculus to the seed.

### Limitations of the study

While *ZFP2* controls SCW synthesis during funiculus development, we cannot rule out that the TF also affects SCW synthesis in other tissues of the developing fruit or seed, which could contribute to aspects of the observed growth defects in the *zfp2* mutants. Additionally, a finer spatio-temporal decomposition of the relationship between eSCW formation in the funiculus and seed loading deficits would likely help us better understand which cell types contribute to the biosynthesis and transport of glucosinolates and fatty acids or their precursors. *ZFP2* directly controls *NST1* to repress SCW formation in the funiculus; however, how *ZFP2* interacts with other key TFs regulating broader fruit development, such as SHATTERPROOF or SEEDSTICK, needs further study. Moreover, it will be interesting to see whether orthologs of *ZFP2* in other plants may play conserved roles in delineating SCW formation at the interface of parenchymatic and vascular tissues.

### RESOURCE AVAILABILITY

#### Lead contact

Further information and requests for resources and reagents should be directed to and will be fulfilled by the lead contact, Wei Ma ([weima@ntu.edu.sg](mailto:weima@ntu.edu.sg)).

### Materials availability

Generated plasmids and seeds are available from the [lead contact](#).

### Data and code availability

- Data: RNA-seq data have been deposited in ArrayExpress (accession number: E-MTAB-14605). Source data for all experiments is available under <https://doi.org/10.5281/zenodo.14342515>.
- Code: all R code to generate the figures and supplemental figures is available under <https://doi.org/10.5281/zenodo.14342515>.
- Any additional information required to reanalyze the data reported in this paper is available from the [lead contact](#) upon request.

### ACKNOWLEDGMENTS

We thank Dr. Hao Yu (National University of Singapore) for the seeds of *N. benthamiana* expressing *H2B-RFP*, Dr. Lisha Shen (Temasek Life Sciences Laboratory), and Dr. Chengxiang Li (Sichuan University) for suggestions on the ChIP-qPCR assay. This work was supported by the Ministry of Education (MOE) of Singapore Tier 2 (grant nos. MOE-T2EP30123-0001 and MOE-T2EP30220-0011 to W.M.), MOE of Singapore Tier 1 (grant no. RG32/23 to W.M.), Villum Investigator (grant no. 25915 to S.P.), DNRF Chair (grant no. DNRF155 to S.P.), Novo Nordisk Laureate (grant no. NNF19OC0056076 to S.P.), Novo Nordisk Emerging Investigator (grant no. NNF20OC0060564 to S.P.), Novo Nordisk Data Science (grant no. NNF0068884 to S.P.), Independent Research Fund Denmark (grant no. 2102-00258B to D.X.), Innovation Fund Denmark (grant no. 3141-00040B to D.X.), Novo Nordisk Foundation (grant no. NNF23OC0085289 to D.X.), MOE of Singapore Tier 2 (grant no. MOE-T2EP30122-0021 to Y.M.), Singapore National Research Foundation Investigatorship (grant no. NRF-NRFI08-2022-0012 to Y.M.), and MOE of Singapore Tier 2 (grant no. MOE-T2EP30122-0017 to M.M.). L.B. is supported by the EMBO postdoctoral fellowship ALTF 37-2022. This work is dedicated to the memory of Dr. John Ohlrogge (Michigan State University), an insightful scientist and great mentor.

### AUTHOR CONTRIBUTIONS

Q.K., L.B., D.X., S.P., and W.M. conceived and designed the experiments. P.M.L., Q.K., L.B., Z.M., Y.Y., T.Q., C.J.R.L., C.C., E.E., J.S.T., W.T.T., and D.X. performed the experiments. P.M.L., Q.K., L.B., Z.M., P.K.L., Y.Y., T.Q., S.K.S., S. Pattanaik, M.M., Y.M., L.Y., D.X., S.P., and W.M. analyzed the data. P.M.L., Q.K., L.B., L.Y., D.X., S.P., and W.M. wrote the manuscript.

### DECLARATION OF INTERESTS

The authors declare no competing interests.

### STAR★METHODS

Detailed methods are provided in the online version of this paper and include the following:

- **KEY RESOURCES TABLE**
- **EXPERIMENTAL MODEL AND STUDY PARTICIPANT DETAILS**
  - Plant materials
  - Accession numbers
- **METHOD DETAILS**
  - Plasmid construction
  - Bioinformatic analysis
  - Gene expression analysis (RNA Extraction, Semi-quantitative RT-PCR, and qRT-PCR)
  - RNA-sequencing (RNA-seq) analysis
  - Histochemical analysis of GUS activity
  - Measurement of silique length, seed weight, seed size and number of seeds per silique
  - Transient expression in *N. benthamiana* and confocal microscopy
  - Histological staining for detection of cell wall components
  - Quantification of funiculus morphology

- Dual-luciferase (dual-LUC) assay
  - Fatty acid analysis
  - Glucosinolate quantification
  - Total lignin quantification
  - ChIP assay
  - Recombinant protein production, purification, and EMSA
- **QUANTIFICATION AND STATISTICAL ANALYSIS**

### SUPPLEMENTAL INFORMATION

Supplemental information can be found online at <https://doi.org/10.1016/j.devcel.2025.01.021>.

Received: June 28, 2024

Revised: November 7, 2024

Accepted: January 31, 2025

Published: February 24, 2025

### REFERENCES

1. Jackson, P. (2010). Food stories: consumption in age of anxiety. *Cult. Geogr.* 17, 147–165.
2. Tan, H., Yang, X., Zhang, F., Zheng, X., Qu, C., Mu, J., Fu, F., Li, J., Guan, R., Zhang, H., et al. (2011). Enhanced seed oil production in canola by conditional expression of Brassica napus LEAFY COTYLEDON1 and LEC1-LIKE in developing seeds. *Plant Physiol.* 156, 1577–1588. <https://doi.org/10.1104/pp.111.175000>.
3. Tan, H., Xiang, X., Tang, J., and Wang, X. (2016). Nutritional functions of the funiculus in Brassica napus seed maturation revealed by transcriptome and dynamic metabolite profile analyses. *Plant Mol. Biol.* 92, 539–553. <https://doi.org/10.1007/s11103-016-0530-3>.
4. Ruuska, S.A., Girke, T., Benning, C., and Ohlrogge, J.B. (2002). Contrapuntal networks of gene expression during *Arabidopsis* seed filling. *Plant Cell* 14, 1191–1206.
5. Agrawal, G.K., and Thelen, J.J. (2006). Large scale identification and quantitative profiling of phosphoproteins expressed during seed filling in oilseed rape. *Mol. Cell. Proteomics* 5, 2044–2059. <https://doi.org/10.1074/mcp.M600084-MCP200>.
6. Baud, S., and Lepiniec, L. (2009). Regulation of de novo fatty acid synthesis in maturing oilseeds of *Arabidopsis*. *Plant Physiol. Biochem.* 47, 448–455. <https://doi.org/10.1016/j.plaphy.2008.12.006>.
7. Santos-Mendoza, M., Dubreucq, B., Baud, S., Parcy, F., Caboche, M., and Lepiniec, L. (2008). Deciphering gene regulatory networks that control seed development and maturation in *Arabidopsis*. *Plant J.* 54, 608–620. <https://doi.org/10.1111/j.1365-313X.2008.03461.x>.
8. Murphy, D.J., and Cummins, I. (1989). Biosynthesis of seed storage products during embryogenesis in rapeseed, Brassica napus. *J. Plant Physiol.* 135, 63–69. [https://doi.org/10.1016/S0176-1617\(89\)80225-1](https://doi.org/10.1016/S0176-1617(89)80225-1).
9. Xu, D., Sanden, N.C.H., Hansen, L.L., Belew, Z.M., Madsen, S.R., Meyer, L., Jørgensen, M.E., Hunziker, P., Veres, D., Crocoll, C., et al. (2023). Export of defensive glucosinolates is key for their accumulation in seeds. *Nature* 617, 132–138. <https://doi.org/10.1038/s41586-023-05969-x>.
10. Millar, J.L., Khan, D., Becker, M.G., Chan, A., Dufresne, A., Sumner, M., and Belmonte, M.F. (2015). Chalazal seed coat development in Brassica napus. *Plant Sci.* 241, 45–54. <https://doi.org/10.1016/j.plantsci.2015.09.019>.
11. Lam, H.M., Coschigano, K., Schultz, C., Melo-Oliveira, R., Tjaden, G., Oliveira, I., Ngai, N., Hsieh, M.H., and Coruzzi, G. (1995). Use of *Arabidopsis* mutants and genes to study amide amino acid biosynthesis. *Plant Cell* 7, 887–898. <https://doi.org/10.1105/tpc.7.7.887>.
12. Khan, D., Millar, J.L., Girard, I.J., Chan, A., Kirkbride, R.C., Pelletier, J.M., Kost, S., Becker, M.G., Yeung, E.C., Stasolla, C., et al. (2015). Transcriptome atlas of the *Arabidopsis* funiculus—a study of maternal seed subregions. *Plant J.* 82, 41–53. <https://doi.org/10.1111/tpj.12790>.

13. Chan, A.C., Khan, D., Girard, I.J., Becker, M.G., Millar, J.L., Sytnik, D., and Belmonte, M.F. (2016). Tissue-specific laser microdissection of the *Brassica napus* funiculus improves gene discovery and spatial identification of biological processes. *J. Exp. Bot.* 67, 3561–3571. <https://doi.org/10.1093/jxb/erw179>.
14. Chan, A., and Belmonte, M.F. (2013). Histological and ultrastructural changes in canola (*Brassica napus*) funicular anatomy during the seed life cycle. *Botany* 91, 671–679. <https://doi.org/10.1139/cjb-2013-0141>.
15. Wang, H.Z., and Dixon, R.A. (2012). On-off switches for secondary cell wall biosynthesis. *Mol. Plant* 5, 297–303. <https://doi.org/10.1093/mp/ssr098>.
16. Zhang, J., Xie, M., Tuskan, G.A., Muchero, W., and Chen, J.G. (2018). Recent advances in the transcriptional regulation of secondary cell wall biosynthesis in the woody plants. *Front. Plant Sci.* 9, 1535. <https://doi.org/10.3389/fpls.2018.01535>.
17. Delmer, D., Dixon, R.A., Keegstra, K., and Mohnen, D. (2024). The plant cell wall—dynamic, strong, and adaptable—is a natural shapeshifter. *Plant Cell* 36, 1257–1311. <https://doi.org/10.1093/plcell/koad325>.
18. Pedersen, G.B., Blaschek, L., Frandsen, K.E.H., Noack, L.C., and Persson, S. (2023). Cellulose synthesis in land plants. *Mol. Plant* 16, 206–231. <https://doi.org/10.1016/j.molp.2022.12.015>.
19. Barros, J., Serk, H., Granlund, I., and Pesquet, E. (2015). The cell biology of lignification in higher plants. *Ann. Bot.* 115, 1053–1074. <https://doi.org/10.1093/aob/mcv046>.
20. Zhong, R., Cui, D., and Ye, Z.H. (2019). Secondary cell wall biosynthesis. *New Phytol.* 221, 1703–1723. <https://doi.org/10.1111/nph.15537>.
21. Rao, X., and Dixon, R.A. (2018). Current models for transcriptional regulation of secondary cell wall biosynthesis in grasses. *Front. Plant Sci.* 9, 399. <https://doi.org/10.3389/fpls.2018.00399>.
22. Nakano, Y., Yamaguchi, M., Endo, H., Rejab, N.A., and Ohtani, M. (2015). NAC-MYB-based transcriptional regulation of secondary cell wall biosynthesis in land plants. *Front. Plant Sci.* 6, 288. <https://doi.org/10.3389/fpls.2015.00288>.
23. Kumar, M., Campbell, L., and Turner, S. (2016). Secondary cell walls: biosynthesis and manipulation. *J. Exp. Bot.* 67, 515–531. <https://doi.org/10.1093/jxb/erv533>.
24. Taylor-Teeples, M., Lin, L., de Lucas, M., Turco, G., Toal, T.W., Gaudinier, A., Young, N.F., Trabucco, G.M., Veling, M.T., Lamothe, R., et al. (2015). An *Arabidopsis* gene regulatory network for secondary cell wall synthesis. *Nature* 517, 571–575. <https://doi.org/10.1038/nature14099>.
25. Mackay, J.P., and Crossley, M. (1998). Zinc fingers are sticking together. *Trends Biochem. Sci.* 23, 1–4. [https://doi.org/10.1016/s0968-0004\(97\)01168-7](https://doi.org/10.1016/s0968-0004(97)01168-7).
26. Ciftci-Yilmaz, S., and Mittler, R. (2008). The zinc finger network of plants. *Cell. Mol. Life Sci.* 65, 1150–1160. <https://doi.org/10.1007/s00018-007-7473-4>.
27. Englbrecht, C.C., Schoof, H., and Böhm, S. (2004). Conservation, diversification and expansion of C2H2 zinc finger proteins in the *Arabidopsis thaliana* genome. *BMC Genomics* 5, 39. <https://doi.org/10.1186/1471-2164-5-39>.
28. Zhou, Z., An, L., Sun, L., Zhu, S., Xi, W., Broun, P., Yu, H., and Gan, Y. (2011). Zinc finger protein5 is required for the control of trichome initiation by acting upstream of zinc finger protein8 in *Arabidopsis*. *Plant Physiol.* 157, 673–682. <https://doi.org/10.1104/pp.111.180281>.
29. Zhou, Z., Sun, L., Zhao, Y., An, L., Yan, A., Meng, X., and Gan, Y. (2013). Zinc Finger Protein 6 (ZFP6) regulates trichome initiation by integrating gibberellin and cytokinin signaling in *Arabidopsis thaliana*. *New Phytol.* 198, 699–708. <https://doi.org/10.1111/nph.12211>.
30. Liu, Y., Liu, D., Hu, R., Hua, C., Ali, I., Zhang, A., Liu, B., Wu, M., Huang, L., and Gan, Y. (2017). AtGIS, a C2H2 zinc-finger transcription factor from *Arabidopsis* regulates glandular trichome development through GA signaling in tobacco. *Biochem. Biophys. Res. Commun.* 483, 209–215. <https://doi.org/10.1016/j.bbrc.2016.12.164>.
31. Yan, A., Wu, M., Zhao, Y., Zhang, A., Liu, B., Schiefelbein, J., and Gan, Y. (2014). Involvement of C2H2 zinc finger proteins in the regulation of epidermal cell fate determination in *Arabidopsis*. *J. Integr. Plant Biol.* 56, 1112–1117. <https://doi.org/10.1111/jipb.12221>.
32. Gan, Y., Kumimoto, R., Liu, C., Ratcliffe, O., Yu, H., and Broun, P. (2006). GLABROUS INFLORESCENCE STEMS modulates the regulation by gibberellins of epidermal differentiation and shoot maturation in *Arabidopsis*. *Plant Cell* 18, 1383–1395. <https://doi.org/10.1105/tpc.106.041533>.
33. Xiao, H., Tang, J., Li, Y., Wang, W., Li, X., Jin, L., Xie, R., Luo, H., Zhao, X., Meng, Z., et al. (2009). STAMENLESS 1, encoding a single C2H2 zinc finger protein, regulates floral organ identity in rice. *Plant J.* 59, 789–801. <https://doi.org/10.1111/j.1365-3113X.2009.03913.x>.
34. Yun, J.Y., Weigel, D., and Lee, I. (2002). Ectopic expression of SUPERMAN suppresses development of petals and stamens. *Plant Cell Physiol.* 43, 52–57. <https://doi.org/10.1093/pcp/pcf018>.
35. Weingartner, M., Subert, C., and Sauer, N. (2011). LATE, a C2H2 zinc-finger protein that acts as floral repressor. *Plant J.* 68, 681–692. <https://doi.org/10.1111/j.1365-3113X.2011.04717.x>.
36. Shang, E., Wang, X., Li, T., Guo, F., Ito, T., and Sun, B. (2021). Robust control of floral meristem determinacy by position-specific multifunctions of KNUCKLES. *Proc. Natl. Acad. Sci. USA* 118, e2102826118. <https://doi.org/10.1073/pnas.2102826118>.
37. Xu, Y., Prunet, N., Gan, E.S., Wang, Y., Stewart, D., Wellmer, F., Huang, J., Yamaguchi, N., Tatsumi, Y., Kojima, M., et al. (2018). SUPERMAN regulates floral whorl boundaries through control of auxin biosynthesis. *EMBO J.* 37, e97499. <https://doi.org/10.15252/embj.201797499>.
38. Han, G., Wei, X., Dong, X., Wang, C., Sui, N., Guo, J., Yuan, F., Gong, Z., Li, X., Zhang, Y., et al. (2020). *Arabidopsis* ZINC FINGER PROTEIN1 acts downstream of GL2 to repress root hair initiation and elongation by directly suppressing bHLH genes. *Plant Cell* 32, 206–225. <https://doi.org/10.1105/tpc.19.00226>.
39. Huang, L., Jiang, Q., Wu, J., An, L., Zhou, Z., Wong, C., Wu, M., Yu, H., and Gan, Y. (2020). Zinc finger protein 5 (ZFP5) associates with ethylene signaling to regulate the phosphate and potassium deficiency-induced root hair development in *Arabidopsis*. *Plant Mol. Biol.* 102, 143–158. <https://doi.org/10.1007/s11103-019-00937-4>.
40. Zhang, H., Ni, L., Liu, Y., Wang, Y., Zhang, A., Tan, M., and Jiang, M. (2012). The C2H2-type zinc finger protein ZFP182 is involved in abscisic acid-induced antioxidant defense in rice. *J. Integr. Plant Biol.* 54, 500–510. <https://doi.org/10.1111/j.1744-7909.2012.01135.x>.
41. Wang, Y., Dou, D., Wang, X., Li, A., Sheng, Y., Hua, C., Cheng, B., Chen, X., Zheng, X., and Wang, Y. (2009). The PsCZF1 gene encoding a C2H2 zinc finger protein is required for growth, development and pathogenesis in *Phytophthora sojae*. *Microb. Pathog.* 47, 78–86. <https://doi.org/10.1016/j.micpath.2009.04.013>.
42. Liu, Y., Khan, A.R., and Gan, Y. (2022). C2H2 zinc finger proteins response to abiotic stress in plants. *Int. J. Mol. Sci.* 23, 2730. <https://doi.org/10.3390/ijms23052730>.
43. Joseph, M.P., Papdi, C., Kozma-Bognár, L., Nagy, I., López-Carbonell, M., Rigó, G., Koncz, C., and Szabados, L. (2014). The *Arabidopsis* ZINC FINGER PROTEIN3 interferes with abscisic acid and light signaling in seed germination and plant development. *Plant Physiol.* 165, 1203–1220. <https://doi.org/10.1104/pp.113.234294>.
44. Weng, L., Zhao, F., Li, R., Xu, C., Chen, K., and Xiao, H. (2015). The zinc finger transcription factor SIZFP2 negatively regulates abscisic acid biosynthesis and fruit ripening in tomato. *Plant Physiol.* 167, 931–949. <https://doi.org/10.1104/pp.114.255174>.
45. Winter, D., Vinegar, B., Nahal, H., Ammar, R., Wilson, G.V., and Provart, N.J. (2007). An "Electronic Fluorescent Pictograph" browser for exploring and analyzing large-scale biological data sets. *PLoS One* 2, e718. <https://doi.org/10.1371/journal.pone.0000718>.
46. Schmid, M., Davison, T.S., Henz, S.R., Pape, U.J., Demar, M., Vingron, M., Schölkopf, B., Weigel, D., and Lohmann, J.U. (2005). A gene expression map of *Arabidopsis thaliana* development. *Nat. Genet.* 37, 501–506. <https://doi.org/10.1038/ng1543>.

47. Mizzotti, C., Rotasperi, L., Moretto, M., Tadini, L., Resentini, F., Galliani, B.M., Galbiati, M., Engelen, K., Pesaresi, P., and Masiero, S. (2018). Time-course transcriptome analysis of *Arabidopsis* siliques discloses genes essential for fruit development and maturation. *Plant Physiol.* *178*, 1249–1268. <https://doi.org/10.1104/pp.18.00727>.
48. Sanden, N.C.H., Kanstrup, C., Crocoll, C., Schulz, A., Nour-Eldin, H.H., Halkier, B.A., and Xu, D. (2024). An UMAMIT-GTR transporter cascade controls glucosinolate seed loading in *Arabidopsis*. *Nat. Plants* *10*, 172–179. <https://doi.org/10.1038/s41477-023-01598-4>.
49. Roeder, A.H.K., and Yanofsky, M.F. (2006). Fruit development in *Arabidopsis*. *Arabidopsis Book* *4*, e0075. <https://doi.org/10.1199/tab.0075>.
50. Balanzà, V., Roig-Villanova, I., Di Marzo, M., Masiero, S., and Colombo, L. (2016). Seed abscission and fruit dehiscence required for seed dispersal rely on similar genetic networks. *Development* *143*, 3372–3381. <https://doi.org/10.1242/dev.135202>.
51. Mitsuda, N., Iwase, A., Yamamoto, H., Yoshida, M., Seki, M., Shinozaki, K., and Ohme-Takagi, M. (2007). NAC transcription factors, NST1 and NST3, are key regulators of the formation of secondary walls in woody tissues of *Arabidopsis*. *Plant Cell* *19*, 270–280. <https://doi.org/10.1105/tpc.106.047043>.
52. Zhang, Q., Xie, Z., Zhang, R., Xu, P., Liu, H., Yang, H., Doblin, M.S., Bacic, A., and Li, L. (2018). Blue light regulates secondary cell wall thickening via MYC2/MYC4 activation of the NST1-directed transcriptional network in *Arabidopsis*. *Plant Cell* *30*, 2512–2528. <https://doi.org/10.1105/tpc.18.00315>.
53. Liu, C., Yu, H., Rao, X., Li, L., and Dixon, R.A. (2021). Abscisic acid regulates secondary cell-wall formation and lignin deposition in *Arabidopsis thaliana* through phosphorylation of NST1. *Proc. Natl. Acad. Sci. USA* *118*, e2010911118. <https://doi.org/10.1073/pnas.2010911118>.
54. Zhong, R., Lee, C., Zhou, J., McCarthy, R.L., and Ye, Z.H. (2008). A battery of transcription factors involved in the regulation of secondary cell wall biosynthesis in *Arabidopsis*. *Plant Cell* *20*, 2763–2782. <https://doi.org/10.1105/tpc.108.061325>.
55. Zhou, J., Lee, C., Zhong, R., and Ye, Z.H. (2009). MYB58 and MYB63 are transcriptional activators of the lignin biosynthetic pathway during secondary cell wall formation in *Arabidopsis*. *Plant Cell* *21*, 248–266. <https://doi.org/10.1105/tpc.108.063321>.
56. Blaschek, L., Murozuka, E., Serk, H., Ménard, D., and Pesquet, E. (2023). Different combinations of laccase paralogs nonredundantly control the amount and composition of lignin in specific cell types and cell wall layers in *Arabidopsis*. *Plant Cell* *35*, 889–909. <https://doi.org/10.1093/plcell/koac344>.
57. Brown, D.M., Zeef, L.A.H., Ellis, J., Goodacre, R., and Turner, S.R. (2005). Identification of novel genes in *Arabidopsis* involved in secondary cell wall formation using expression profiling and reverse genetics. *Plant Cell* *17*, 2281–2295. <https://doi.org/10.1105/tpc.105.031542>.
58. Jensen, J.K., Kim, H., Cocuron, J.C., Orlor, R., Ralph, J., and Wilkerson, C.G. (2011). The DUF579 domain containing proteins IRX15 and IRX15-L affect xylan synthesis in *Arabidopsis*. *Plant J.* *66*, 387–400. <https://doi.org/10.1111/j.1365-3113X.2010.04475.x>.
59. Fernández-Pérez, F., Pomar, F., Pedreño, M.A., and Novo-Uzal, E. (2015). The suppression of AtPrx52 affects fibers but not xylem lignification in *Arabidopsis* by altering the proportion of syringyl units. *Physiol. Plant.* *154*, 395–406. <https://doi.org/10.1111/ppl.12310>.
60. Kong, Q., Low, P.M., Lim, A.R.Q., Yang, Y., Yuan, L., and Ma, W. (2022). Functional antagonism of WRI1 and TCP20 modulates GH3.3 expression to maintain auxin homeostasis in roots. *Plants (Basel)* *11*, 454. <https://doi.org/10.3390/plants11030454>.
61. Lim, A.R.Q., Kong, Q., Singh, S.K., Guo, L., Yuan, L., and Ma, W. (2022). Sunflower WRINKLED1 plays a key role in transcriptional regulation of oil biosynthesis. *Int. J. Mol. Sci.* *23*, 3054. <https://doi.org/10.3390/ijms23063054>.
62. Yang, Y., Kong, Q., Tee, W.T., Li, Y., Low, P.M., Patra, B., Guo, L., Yuan, L., and Ma, W. (2023). Transcription factor bZIP52 modulates *Arabidopsis* seed oil biosynthesis through interaction with WRINKLED1. *Plant Physiol.* *192*, 2628–2639. <https://doi.org/10.1093/plphys/kiad270>.
63. Mitsuda, N., and Ohme-Takagi, M. (2009). Functional analysis of transcription factors in *Arabidopsis*. *Plant Cell Physiol.* *50*, 1232–1248. <https://doi.org/10.1093/pcp/pcp075>.
64. Hiratsu, K., Mitsuda, N., Matsui, K., and Ohme-Takagi, M. (2004). Identification of the minimal repression domain of SUPERMAN shows that the DLELRL hexapeptide is both necessary and sufficient for repression of transcription in *Arabidopsis*. *Biochem. Biophys. Res. Commun.* *321*, 172–178. <https://doi.org/10.1016/j.bbrc.2004.06.115>.
65. Ohta, M., Matsui, K., Hiratsu, K., Shinshi, H., and Ohme-Takagi, M. (2001). Repression domains of class II ERF transcriptional repressors share an essential motif for active repression. *Plant Cell* *13*, 1959–1968. <https://doi.org/10.1105/tpc.010127>.
66. Yang, J., Liu, Y., Yan, H., Tian, T., You, Q., Zhang, L., Xu, W., and Su, Z. (2018). PlantEAR: functional analysis platform for plant EAR motif-containing proteins. *Front. Genet.* *9*, 590. <https://doi.org/10.3389/fgene.2018.00590>.
67. Sadowski, I., Ma, J., Triezenberg, S., and Ptashne, M. (1988). GAL4-VP16 is an unusually potent transcriptional activator. *Nature* *335*, 563–564. <https://doi.org/10.1038/335563a0>.
68. Kubo, K., Sakamoto, A., Kobayashi, A., Rybka, Z., Kanno, Y., Nakagawa, H., and Takatsui, H. (1998). Cys2/His2 zinc-finger protein family of petunia: evolution and general mechanism of target-sequence recognition. *Nucleic Acids Res.* *26*, 608–615. <https://doi.org/10.1093/nar/26.2.608>.
69. Sun, B., Zhou, Y., Cai, J., Shang, E., Yamaguchi, N., Xiao, J., Looi, L.S., Wee, W.Y., Gao, X., Wagner, D., et al. (2019). Integration of transcriptional repression and Polycomb-mediated silencing of WUSCHEL in floral meristems. *Plant Cell* *31*, 1488–1505. <https://doi.org/10.1105/tpc.18.00450>.
70. Kagale, S., and Rozwadowski, K. (2011). EAR motif-mediated transcriptional repression in plants: an underlying mechanism for epigenetic regulation of gene expression. *Epigenetics* *6*, 141–146. <https://doi.org/10.4161/epi.6.2.13627>.
71. Causier, B., Ashworth, M., Guo, W., and Davies, B. (2012). The TOPLESS interactome: a framework for gene repression in *Arabidopsis*. *Plant Physiol.* *158*, 423–438. <https://doi.org/10.1104/pp.111.186999>.
72. Wang, H., Avci, U., Nakashima, J., Hahn, M.G., Chen, F., and Dixon, R.A. (2010). Mutation of WRKY transcription factors initiates pith secondary wall formation and increases stem biomass in dicotyledonous plants. *Proc. Natl. Acad. Sci. USA* *107*, 22338–22343. <https://doi.org/10.1073/pnas.1016436107>.
73. Crawford, B.C.W., and Yanofsky, M.F. (2008). The formation and function of the female reproductive tract in flowering plants. *Curr. Biol.* *18*, R972–R978. <https://doi.org/10.1016/j.cub.2008.08.010>.
74. Zhang, Y., Fan, S., Hua, C., Teo, Z.W.N., Kiang, J.X., Shen, L., and Yu, H. (2022). Phase separation of HRLP regulates flowering time in *Arabidopsis*. *Sci. Adv.* *8*, eabn5488. <https://doi.org/10.1126/sciadv.abn5488>.
75. Kumar, S., Stecher, G., Li, M., Niyaz, C., and Tamura, K. (2018). MEGA X: Molecular evolutionary genetics analysis across computing platforms. *Mol. Biol. Evol.* *35*, 1547–1549. <https://doi.org/10.1093/molbev/msy096>.
76. Letunic, I., Khedkar, S., and Bork, P. (2021). SMART: recent updates, new developments and status in 2020. *Nucleic Acids Res.* *49*, D458–D460. <https://doi.org/10.1093/nar/gkaa937>.
77. Thompson, J.D., Higgins, D.G., and Gibson, T.J. (1994). Clustal W: improving the sensitivity of progressive multiple sequence alignment through sequence weighting, position-specific gap penalties and weight matrix choice. *Nucleic Acids Res.* *22*, 4673–4680. <https://doi.org/10.1093/nar/22.22.4673>.
78. Love, M.I., Huber, W., and Anders, S. (2014). Moderated estimation of fold change and dispersion for RNA-seq data with DESeq2. *Genome Biol.* *15*, 550. <https://doi.org/10.1186/s13059-014-0550-8>.
79. Wolny, A., Cerrone, L., Vijayan, A., Tofaneli, R., Barro, A.V., Louveaux, M., Wenzl, C., Strauss, S., Wilson-Sánchez, D., Lymbouridou, R., et al. (2020).

- Accurate and versatile 3D segmentation of plant tissues at cellular resolution. *eLife* 9, e57613. <https://doi.org/10.7554/eLife.57613>.
80. Legland, D., Arganda-Carreras, I., and Andrey, P. (2016). MorphoLibJ: integrated library and plugins for mathematical morphology with ImageJ. *Bioinformatics* 32, 3532–3534. <https://doi.org/10.1093/bioinformatics/btw413>.
81. Ahlers, J., Althviz Moré, D., Amsalem, O., Anderson, A., Bokota, G., Boone, P., Bragantini, J., Buckley, G., Burt, A., Bussonnier, M., et al. (2023). Napari: A Multi-dimensional Image Viewer for Python, [v0.4.18] (Zenodo). 10.5281/zenodo.8115575.
82. Wickham, H., Averick, M., Bryan, J., Chang, W., McGowan, L.D., François, R., Grolemund, G., Hayes, A., Henry, L., Hester, J., et al. (2019). Welcome to the tidyverse. *J. Open Source Software* 4, 1686. <https://doi.org/10.21105/joss.01686>.
83. Ma, W., Kong, Q., Arondel, V., Kilaru, A., Bates, P.D., Thrower, N.A., Benning, C., and Ohlrogge, J.B. (2013). Wrinkled1, a ubiquitous regulator in oil accumulating tissues from *Arabidopsis* embryos to oil palm mesocarp. *PLoS One* 8, e68887. <https://doi.org/10.1371/journal.pone.0068887>.
84. Hellens, R.P., Allan, A.C., Friel, E.N., Bolitho, K., Grafton, K., Templeton, M.D., Karunairetnam, S., Gleave, A.P., and Laing, W.A. (2005). Transient expression vectors for functional genomics, quantification of promoter activity and RNA silencing in plants. *Plant Methods* 1, 13. <https://doi.org/10.1186/1746-4811-1-13>.
85. Cheng, C.Y., Krishnakumar, V., Chan, A.P., Thibaud-Nissen, F., Schobel, S., and Town, C.D. (2017). Araport11: a complete reannotation of the *Arabidopsis thaliana* reference genome. *Plant J.* 89, 789–804. <https://doi.org/10.1111/tpj.13415>.
86. Bray, N.L., Pimentel, H., Melsted, P., and Pachter, L. (2016). Near-optimal probabilistic RNA-seq quantification. *Nat. Biotechnol.* 34, 525–527. <https://doi.org/10.1038/nbt.3519>.
87. Benjamini, Y., and Hochberg, Y. (1995). Controlling the false discovery rate: A practical and powerful approach to multiple testing. *J. R. Stat. Soc. B Methodol.* 57, 289–300. <https://doi.org/10.1111/j.2517-6161.1995.tb02031.x>.
88. The Gene Ontology Consortium (2019). The Gene Ontology Resource: 20 years and still GOing strong. *Nucleic Acids Res.* 47, D330–D338. <https://doi.org/10.1093/nar/gky1055>.
89. Falcon, S., and Gentleman, R. (2008). Hypergeometric testing used for gene set enrichment analysis. In *Bioconductor Case Studies* (Springer), pp. 207–220. [https://doi.org/10.1007/978-0-387-77240-0\\_14](https://doi.org/10.1007/978-0-387-77240-0_14).
90. Yu, G., Wang, L.-G., Han, Y., and He, Q.-Y. (2012). clusterProfiler: an R package for comparing biological themes among gene clusters. *OMICS A J. Integr. Biol.* 16, 284–287. <https://doi.org/10.1089/omi.2011.0118>.
91. Jefferson, R.A., Kavanagh, T.A., and Bevan, M.W. (1987). GUS fusions: beta-glucuronidase as a sensitive and versatile gene fusion marker in higher plants. *EMBO J.* 6, 3901–3907. <https://doi.org/10.1002/j.1460-2075.1987.tb02730.x>.
92. Ursache, R., Andersen, T.G., Marhavý, P., and Geldner, N. (2018). A protocol for combining fluorescent proteins with histological stains for diverse cell wall components. *Plant J.* 93, 399–412. <https://doi.org/10.1111/tpj.13784>.
93. Blaschek, L., Champagne, A., Dimotakis, C., Nuoendagula, D., Decou, R., Hishiyama, S., Kratzer, S., Kajita, S., and Pesquet, E. (2020). Cellular and genetic regulation of coniferaldehyde incorporation in lignin of herbaceous and woody plants by quantitative Wiesner staining. *Front. Plant Sci.* 11, 109. <https://doi.org/10.3389/fpls.2020.00109>.
94. Lim, A.R.Q., Kong, Q., Noor, A., Song, Y.Q., Pattanaik, S., Yuan, L., and Ma, W. (2023). B-BOX-DOMAIN PROTEIN32 modulates seed oil biosynthesis in *Arabidopsis* by interacting with WRINKLED1. *Plant Physiol.* 193, 919–922. <https://doi.org/10.1093/plphys/kiad419>.
95. Crocoll, C., Halkier, B.A., and Burow, M. (2016). Analysis and quantification of glucosinolates. *Curr. Protoc. Plant Biol.* 1, 385–409. <https://doi.org/10.1002/cppb.20027>.
96. Barnes, W.J., and Anderson, C.T. (2017). Acetyl bromide soluble lignin (ABSL) assay for total lignin quantification from plant biomass. *Bio Protoc.* 7, e2149. <https://doi.org/10.21769/BioProtoc.2149>.
97. Yamaguchi, N., Winter, C.M., Wu, M.F., Kwon, C.S., William, D.A., and Wagner, D. (2014). PROTOCOLS: chromatin immunoprecipitation from *Arabidopsis* tissues. *Arabidopsis Book* 12, e0170. <https://doi.org/10.1199/tab.0170>.
98. Kong, Q., Pattanaik, S., Feller, A., Werkman, J.R., Chai, C., Wang, Y., Grotewold, E., and Yuan, L. (2012). Regulatory switch enforced by basic helix-loop-helix and ACT-domain mediated dimerizations of the maize transcription factor R. *Proc. Natl. Acad. Sci. USA* 109, E2091–E2097. <https://doi.org/10.1073/pnas.1205513109>.

STAR★METHODS

KEY RESOURCES TABLE

REAGENT or RESOURCE	SOURCE	IDENTIFIER
<b>Bacterial and Virus Strains</b>		
<i>Agrobacterium tumefaciens</i>	N/A	GV3101
<i>Agrobacterium tumefaciens</i>	N/A	AGL1
<i>Escherichia coli</i>	N/A	DH5 $\alpha$
<i>Escherichia coli</i>	N/A	BL21(DE3) Rosetta
<b>Chemicals, Peptides, and Recombinant Proteins</b>		
Sulfuric acid	Sigma-Aldrich	Cat#258105
Chloroform >99.8%	Fisher Scientific	Cat#C/4960/17
Pierce Protease inhibitor tablets (EDTA free)	ThermoFisher Scientific	Cat#A32965
Imidazole	Sigma	Cat#I0250-250G
Pierce Universal Nuclease for Cell Lysis	ThermoFisher Scientific	Cat#88702
Lysozyme from chicken egg white	Sigma-Aldrich	Cat#L3970
CellLytic B Cell Lysis Reagent	Sigma-Aldrich	Cat#C8740
X-gluc (CHX salt)	GoldBio	Cat#G1281C
Butylated hydroxytoluene (BHT)	Sigma-Aldrich	Cat#W218405
Toluene	Sigma-Aldrich	Cat#34866
Hexane	Fisher Scientific	Cat#H292-4
Glyceryl triheptadecanoate	ChemCruz	Cat#sc-215086A
Formaldehyde solution	Sigma-Aldrich	Cat#252549
Protein G Magnetic Beads	ThermoFisher Scientific	Cat#88847
Salmon sperm DNA	ThermoFisher Scientific	Cat#15632011
anti-flag antibody	Proteintech	Cat#20543-1-AP
GST-6xHis-ZFP2	This paper	N/A
Methanol $\geq$ 99.9%	VWR	Cat#85681.320
p-Hydroxybenzylglucosinolate potassium salt	Extrasynthese	Cat#2511S
DEAS-Sephadex A-25	Cytiva	Cat#17017002
Sulfatase Type H-1	Sigma-Aldrich	Cat#9626
Acetyl Bromide	Sigma-Aldrich	Cat#135968
Acetic Acid, glacial	Merck	Cat#1.00063
Sodium Hydroxide	Sigma-Aldrich	Cat#S5881
Hydroxylamine Hydrochloride	Sigma-Aldrich	Cat#431362
Xylitol	Sigma-Aldrich	Cat#W507930
Sodium deoxycholate	Sigma-Aldrich	Cat#D6750
Urea	Sigma-Aldrich	Cat#U5378
Basic fuchsin	Merck	CAS#632-99-5
Fluorescent Brightener 28 (Calcofluor White)	ICN	CAS#4404-43-7
Phloroglucinol	Sigma-Aldrich	Cat#P3502
Hydrochloric acid	Supelco	Cat#1.01834
<b>Critical commercial assays</b>		
Dual-Luciferase® Reporter Assay System	Promega	Cat#E1910
Monarch® Total RNA Miniprep Kit	New England Biolabs	Cat#T2010S
LunaScript® RT SuperMix Kit	New England Biolabs	Cat#E3010
NEBNext® Ultra™ II Directional RNA Library Prep Kit for Illumina®	New England Biolabs	Cat#E7760S
Luna® Universal qPCR Master Mix	New England Biolabs	Cat#M3003

(Continued on next page)

**Continued**

REAGENT or RESOURCE	SOURCE	IDENTIFIER
Monarch PCR & DNA cleanup kit	New England Biolabs	Cat#T1030L
Chemiluminescent Nucleic Acid Detection Module Kit	ThermoFisher Scientific	Cat#89880
<b>Experimental Models: Organisms/Strains</b>		
<i>Arabidopsis thaliana</i> : <i>zfp2-1</i>	ABRC	N/A
<i>Arabidopsis thaliana</i> : <i>zfp2-2</i>	ABRC	N/A
<i>Arabidopsis thaliana</i> : <i>zfp2-3</i>	ABRC	N/A
<i>Arabidopsis thaliana</i> : <i>nst1-1</i>	ABRC	N/A
<i>Arabidopsis thaliana</i> : <i>proZFP2:GUS</i> in Col-0	This paper	N/A
<i>Arabidopsis thaliana</i> : <i>proZFP2:FLAG-ZFP2-YFP</i> in <i>zfp2-2</i>	This paper	N/A
<i>Arabidopsis thaliana</i> : <i>proNST1:GUS</i> in Col-0	This paper	N/A
<i>Arabidopsis thaliana</i> : <i>proNST1:GUS</i> in <i>zfp2-2</i>	This paper	N/A
<i>Nicotiana benthamiana</i> : wild-type with <i>H2B-RFP</i>	Zhang et al. <sup>74</sup>	N/A
<b>Recombinant DNA</b>		
pGWB3:pZFP2	This paper	N/A
pEarleyGate100:ZFP2 and its mutants	This paper	N/A
pEarleyGate100:ZFP2-VP16	This paper	N/A
pEarleyGate100:proZFP2:FLAG-ZFP2-YFP	This paper	N/A
pGreenII 0800-LUC:proNST1	This paper	N/A
pGreenII 0800-LUC:proMYB63	This paper	N/A
pGreenII 0800-LUC:proSND2	This paper	N/A
pNIC-GST:ZFP2 (GST-6xHis-ZFP2)	This paper	N/A
<b>Oligonucleotides</b>		
Primers for plasmid construction (see Table S1)	This paper	N/A
Quantitative real-time PCR primers (see Table S2)	This paper	N/A
Chromatin-immunoprecipitation PCR primers (see Table S3)	This paper	N/A
Semi-quantitative reverse transcription-PCR primers (see method)	This paper	N/A
EMSA probes (see method)	This paper	N/A
<b>Software and Algorithms</b>		
ImageJ	NIH	<a href="https://imagej.nih.gov/ij/index.html">https://imagej.nih.gov/ij/index.html</a>
MEGA X	Kumar et al. <sup>75</sup>	<a href="http://www.megasoftware.net">www.megasoftware.net</a>
Simple Modular Architecture Research Tool (SMART)	Letunic et al. <sup>76</sup>	<a href="https://smart.embl.de">https://smart.embl.de</a>
CLUSTAL W	Thompson et al. <sup>77</sup>	<a href="https://www.genome.jp/tools-bin/clustalw">https://www.genome.jp/tools-bin/clustalw</a>
R package DESeq2	Love et al. <sup>78</sup>	<a href="https://bioconductor.org/packages/release/data/annotation/html/org.At.tair.db.html">https://bioconductor.org/packages/release/data/annotation/html/org.At.tair.db.html</a>
PlantSeg (1.6.2)	Wolny et al. <sup>79</sup>	<a href="https://github.com/kreshuklab/plant-seg">https://github.com/kreshuklab/plant-seg</a>
MorpholibJ (1.6.3)	Legland et al. <sup>80</sup>	<a href="https://github.com/ijpb/MorphoLibJ">https://github.com/ijpb/MorphoLibJ</a>
Napari (0.4.18)	Ahlers et al. <sup>81</sup>	<a href="https://github.com/napari/napari">https://github.com/napari/napari</a>
R package 'tidyverse' (2.0.0)	Wickham et al. <sup>82</sup>	<a href="https://www.tidyverse.org">https://www.tidyverse.org</a>
<b>Deposited Data</b>		
R code and source data to reproduce the figures	This paper	<a href="https://doi.org/10.5281/zenodo.14342515">https://doi.org/10.5281/zenodo.14342515</a>

## EXPERIMENTAL MODEL AND STUDY PARTICIPANT DETAILS

### Plant materials

*Arabidopsis* (*Arabidopsis thaliana*) WT (Columbia ecotype) was used in this study. *Arabidopsis*, *Nicotiana benthamiana*, and transgenic *N. benthamiana* expressing *H2B-RFP*<sup>74</sup> plants were grown in a growth chamber at 23 °C with a photoperiod of 16 h light (100–150  $\mu\text{mol m}^{-2} \text{sec}^{-1}$  illumination)/8 h dark. *Arabidopsis* transformation, seed sterilization, plant growth, and selection of homozygous transgenic lines were performed as described previously.<sup>62,83</sup> Seeds of *zfp2-1* (SALK\_006473), *zfp2-2* (SALK\_060453), *zfp2-3* (SALK\_007343), and *nst1-1* (SALK\_120377C) mutants were obtained from the *Arabidopsis* Biological Resource Center (ABRC). The double mutant *zfp2-2 nst1-1* was generated by crossing *zfp2-2* with *nst1-1*.

### Accession numbers

Sequence information are identified in The *Arabidopsis* Information Resource database ([www.arabidopsis.org](http://www.arabidopsis.org)), under accession numbers: ZFP2 (AT5G57520); NST1 (AT2G46770); MYB63 (AT1G79180); SND2 (AT1G79180); LAC17 (AT5G60020); IRX9 (AT2G37090); IRX15 (AT2G37090); LAC12 (AT5G05390); PRX52 (AT5G05340); IPP2 (AT3G02780); ACTIN2 (AT3G18780); ZFP1 (AT1G80730); ZFP4 (AT1G66140); ZFP7 (AT1G24625); AT5G10970; ZFP3 (AT5G25160); AT5G01860; KNU (AT5G14010); LATE (AT5G48890); GIS (AT3G58070); ZFP8 (AT2G41940); GIS2 (AT5G06650); ZFP5 (AT1G10480); GIS3 (AT1G68360); ZFP6 (AT1G67030); AT5G05120; TAC1 (AT3G09290); RBE (AT5G06070); SUP (AT3G23130); ZP1 (AT4G17810); ZFP10 (AT2G37740); ZFP11 (AT2G42410); JAG (AT1G68480); AT5G54360; AT5G27880, as well as in Ensembl Plants (<https://plants.ensembl.org/index.html>), PANTHER (<https://pantherdb.org/>) and PLAZA database ([https://bioinformatics.psb.ugent.be/plaza/versions/plaza\\_v5\\_dicots/](https://bioinformatics.psb.ugent.be/plaza/versions/plaza_v5_dicots/)) under accession numbers: BnZFP2 (CDY11864); CsZFP2 (Csa11g091100.1); GmZFP2 (KRH02887); ZmZFP2 (Zm00001eb320440); OsZFP2 (Os08g0555700).

## METHOD DETAILS

### Plasmid construction

For the generation of transgenic GUS line, 1.5 kb promoter sequence upstream of the start codon of *ZFP2* and 2 kb promoter sequence upstream of the start codon of *NST1* was amplified from *Arabidopsis* WT genomic DNA (gDNA) and introduced into pENTR4 entry vector, and then subcloned into pGWB3 vector using the LR reaction kit (Life Technologies). Entry construct of *ZFP2* was obtained from ABRC. Truncated variants and site-directed mutants of *ZFP2* [*ZFP2*<sup>1-143</sup>, *ZFP2*<sup>28-143</sup>, *ZFP2*<sup>L144A/L146A/L148A/L150A</sup> (*ZFP2* mEAR3)], as well as *ZFP2*-VP16 was amplified through PCR and subcloned into entry vector. *ZFP2*<sup>L9A/L11A/L13A/L21A/L23A/L25A/L27A/L144A/L146A/L148A/L150A</sup> (*ZFP2* mEAR1-3) and *ZFP2*<sup>L67H/G69V</sup>, were synthesized to pTwist ENTR vector by Twist Bioscience to achieve entry constructs. The entry constructs of *ZFP2* and variants were introduced into pEarleyGate binary vectors through LR reactions. 2 kb promoter sequences upstream of the start codon of *NST1*, *MYB63* and *SND2* were amplified using *Arabidopsis* WT gDNA and subcloned into pGreenII 0800-LUC vector.<sup>84</sup> For protein expression, full-length coding sequence of *ZFP2* was introduced into pNIC-GST vector (Protein Production Platform, Nanyang Technological University). For the construct of *proZFP2:FLAG-ZFP2-YFP*, the 1.5 kb promoter sequence upstream of *ZFP2* start codon was amplified by PCR. The amplified *ZFP2* promoter sequence was fused with *FLAG*, *ZFP2* and *YFP* sequences and introduced into pENTR4 vector, and subsequently subcloned into pEarleyGate100 through LR reactions. Primers used in the plasmid construction in this study are provided in [Table S1](#).

### Bioinformatic analysis

MEGA X software<sup>75</sup> was used for the construction of a phylogenetic tree through the neighbor-joining method with bootstrap values set at 1000 replicates. Domains predictions were conducted by Simple Modular Architecture Research Tool (SMART).<sup>76</sup> Protein sequence alignment was analyzed by CLUSTAL W program.<sup>77</sup>

### Gene expression analysis (RNA Extraction, Semi-quantitative RT-PCR, and qRT-PCR)

Plant materials were harvested and immediately frozen in liquid nitrogen and stored at -80°C freezer until use for RNA extraction. Total RNA was extracted using the Monarch Total RNA Miniprep Kit (New England Biolabs) according to the supplier's instructions. First-strand cDNA was synthesized using the LunaScript RT SuperMix Kit (New England Biolabs). Semi-quantitative reverse transcription-PCR (RT-PCR) was performed using GoTaq Green 2X Master Mix (Promega). *ACTIN2* (*ACT2*) gene was used as an internal control, with following gene-specific primers [forward (FW), 5'-GCTCCCAGGGCTGTTTTTCCCA-3', and reverse (RV), 5'-CCC GCTCTGCTGTTGTGTTGA-3']. Primers for *ZFP2* (FW, 5'-CTACCAGCCAAACACATCCCT-3', and RV, 5'-CGCGTCGACTTAGA GCCTTAAGGATAA-3'). Quantitative real-time PCR (qRT-PCR) was conducted using Luna Universal qPCR Master Mix (New England Biolabs) according to the supplier's instructions. *IPP2* gene was used as an internal control to normalize the gene expression. The primers used for qRT-PCR are provided in [Table S2](#).

### RNA-sequencing (RNA-seq) analysis

Total RNA extracted from pooled *Arabidopsis* siliques 12 days after pollination (DAP) were used for the assay, with 3 biological replicates each for WT and *zfp2-2*. Sample RNA concentration, integrity, and purity were evaluated using Nanodrop, agarose electrophoresis, and Agilent 2100 Bioanalyzer. For each sample, RNA-seq libraries were generated using NEBNext Ultra II Directional RNA

Library Prep Kit for Illumina and sequenced with Illumina Novaseq-6000 using paired-end sequencing with read lengths of 150 base pairs at sequencing depths of ~2 million reads per sample. For expression quantification and *in silico* quality control of RNA-seq data, 27,445 coding sequences from primary transcripts of the *A. thaliana* nuclear genome<sup>85</sup> downloaded from The *Arabidopsis* Information Resource used as read pseudoalignment references using Kallisto,<sup>86</sup> in order to estimate the gene expression. TPM (transcript per million)-normalized abundance values of genes calculated from Kallisto were mean-centered, and standardized to unit variance within samples, and used as features for Principal component analysis (PCA) to visualize global transcriptome similarity between samples. For differential gene expression analysis and gene-ontology enrichment analysis, un-normalized gene counts of samples estimated by Kallisto were used to detect gene differential expression in *zfp2-2* siliques using the R package DESeq2,<sup>78</sup> with WT samples designated as control. To identify differentially expressed genes (DEGs), genes with a Benjamini-Hochberg<sup>87</sup> corrected p-value of  $\leq 0.05$  from DESeq2's Wald tests, and a Log2FC of  $\geq 1$  or  $\leq -1$  were considered to be significantly upregulated and downregulated DEGs respectively. Functional annotations of *Arabidopsis thaliana* genes in the form of biological process (BP) Gene-ontology (GO) terms<sup>88</sup> were imported from the R package 'org.At.tair.db' (<https://bioconductor.org/packages/release/data/annotation/html/org.At.tair.db.html>). Using hypergeometric tests<sup>89</sup> onboard the R package ClusterProfiler,<sup>90</sup> BP GO terms that were statistically overrepresented (enriched) in upregulated DEGs were identified using a BH corrected p-value threshold of  $\leq 0.01$ . The list of enriched terms was simplified by removing terms that had more than 70% overlap with higher ranked terms.

### Histochemical analysis of GUS activity

Histochemical analysis of  $\beta$ -glucuronidase (*GUS*) reporter activity was conducted according to a method previously described.<sup>91</sup> Homozygous transgenic plants of *proZFP2:GUS* were used for this assay. Developing siliques were harvested and incubated in 1X PBS buffer containing 1 mM 5-bromo-4-chloroindoyl- $\beta$ -D-glucuronide (X-Gluc), 10 mM EDTA and 0.1% Triton X-100 overnight at 37 °C. To examine GUS activity in the funiculus, the silique valves were removed. Tissues were cleared in acetic acid:ethanol (3:1) solution overnight and then stored in 70% ethanol the next day. Images were taken under a Leica stereomicroscope.

### Measurement of silique length, seed weight, seed size and number of seeds per silique

*Arabidopsis* seed weight and size were measured according to a protocol described previously,<sup>62</sup> with slight changes. A sample size of 100 and 120 mature seeds (dried for at least a week after harvesting) were used respectively. For silique length, a sample size of 28–33 siliques at 7 DAP were harvested. Images were captured using an Epson Perfection V600 Photo scanner. ImageJ was used to measure length of siliques and seeds, as well as width, area, and perimeter of seeds. As for seeds per silique quantification, mature and intact siliques (around stage 18<sup>49</sup>) were harvested to count the number of seeds per silique.

### Transient expression in *N. benthamiana* and confocal microscopy

Agrobacterium-mediated transient expression in *N. benthamiana* and confocal microscopy imaging in *N. benthamiana* leaves were performed as previously described<sup>60,62</sup> with slight modifications. *Agrobacterium tumefaciens* cells were resuspended in MMA medium [10 mM MES, pH 5.6, 10 mM MgCl<sub>2</sub>, 100  $\mu$ M acetosyringone] to an OD<sub>600</sub> of 1.2. The cells were incubated for 3–4 h at room temperature and adjusted to an OD<sub>600</sub> 0.2, before infiltrating into the leaves of *N. benthamiana*. The plasmid pEAQ HT producing P19 was co-infiltrated with the constructs. Healthy leaves of *N. benthamiana* were infiltrated with *A. tumefaciens* suspensions via a 1 mL blunt-end syringe. After agroinfiltration, *N. benthamiana* plants were placed in a growth chamber for 2–3 days. To investigate the subcellular localization of ZFP2, the *N. Benthamiana* leaf epidermal cells transiently expressing YFP-ZFP2 were observed under Zeiss LSM 980 confocal laser scanning microscope (CLSM) equipped with a Zeiss Alpha Plan Apochromat 63x, NA 1.40 oil objective. The YFP/RFP signal were excited by argon lasers at 509 nm/561 nm and collected at 505–570 nm/570–650 nm, respectively. The same microscope set up on recording YFP was applied on imaging the ZFP2-YFP in the siliques of transgenic *zfp2-2* (*proZFP2:FLAG-ZFP2-YFP* in *zfp2-2*), of which the valves were peeled off to expose the developing seeds and funiculus. Z-stack image with 0.4  $\mu$ m step size was applied to scan the whole funiculus. The final image was maximum projected to present the YFP signal.

### Histological staining for detection of cell wall components

Siliques were harvested in late stage 17,<sup>49</sup> 11–12 DAP, when elongation and lignification were complete but before turning yellow. Siliques were stored in 70% ethanol at -20°C until further use. For imaging, siliques were cleared overnight in ClearSee (10% xylitol, 15% sodium deoxycholate, 25% urea in H<sub>2</sub>O). Cleared siliques were stained with basic fuchsin (0.001% in ClearSee) to label lignin and calcofluor white (Fluorescent Brightener 28, ICN Biomed; 0.01% in ClearSee) to label cellulose according to Ursache et al.<sup>92</sup> Valves and septum/replum, which generally separated during the clearing and staining procedure, were mounted between glass slide and cover slip in ClearSee, using a thin layer of vacuum grease around the sample to prevent crushing the tissue. Silique cross-sections of 50  $\mu$ m thickness were cut with a Leica VT1000 S Vibrating blade microtome and stained/mounted as described above. Imaging was performed using a Leica SP-5X inverted confocal laser scanning microscope, equipped with a 63x water objective (NA 1.2). Calcofluor white fluorescence was observed using 405 nm excitation and emission between 425 and 475 nm. Basic Fuchsin fluorescence was observed at 561 nm excitation and emission between 570 and 625 nm. Images were acquired with voxel dimensions of 240  $\times$  240  $\times$  250 nm (x  $\times$  y  $\times$  z). Images were visualized and analyzed in Fiji.

Wiesner staining of ethanol-cleared 11–12 DAP siliques was performed as previously described,<sup>93</sup> with slight modifications. Valves were removed from the septum with tweezers, the septum was placed on a glass slide and mounted in Wiesner reagent (1%

phloroglucinol in ethanol:12 M HCl:MilliQ, 1:1:1). Images were acquired between 2 and 15 min after staining using a Keyence VHX-7000 with focus stacking.

### Quantification of funiculus morphology

The density of cortex cells forming ectopic SCWs was counted manually in 11–12 DAP old funiculi, dividing the number of non-xylem cells with a lignified SCW by the observed length of the funiculus. To measure cell lengths in funiculi, the calcofluor channel was segmented in three dimensions with PlantSeg (v 1.6.0; GASP segmentation, 'generic\_confocal\_3D\_unet').<sup>79</sup> Segmented cells touching the border of the 3D stack or outside the biologically plausible range of around 300–2000  $\mu\text{m}^3$  were filtered out. 3D ellipsoids were fitted to the segmented cells and the radius of the long axis was measured using the MorpholibJ ImageJ plugin.<sup>80</sup> Segmented cells were visualized and colored according to long axis diameter in Napari.<sup>81</sup>

### Dual-luciferase (dual-LUC) assay

Dual-LUC assays in *N. benthamiana* leaves were conducted as described previously.<sup>60,94</sup> The dual-LUC assay was performed using Dual-Luciferase Reporter 1000 Assay System (Promega). After agroinfiltration, *N. benthamiana* plants were placed in a growth chamber for 3 days. To harvest the samples for the assay, three leaf discs (5–6 mm in diameter) were excised and ground in liquid nitrogen (to fine powder) and homogenized in 100  $\mu\text{L}$  Passive Lysis buffer. Subsequently, 40  $\mu\text{L}$  Luciferase Assay Buffer was added to 5  $\mu\text{L}$  of the crude extract, and the firefly LUC activity was measured by a cell imaging multimode plate reader (BioTek Cytation 5). 40  $\mu\text{L}$  Stop and Glow Buffer was then added and the Renilla (REN) LUC activity was measured. To quantify the relative luciferase activity, the firefly LUC activity was normalized against the REN LUC activity.

### Fatty acid analysis

Lipid analysis in *Arabidopsis* mature seeds was conducted as previously described.<sup>83</sup> For lipid analysis in developing seeds, 15 harvested *Arabidopsis* developing seeds were stored in a glass tube with 1 mL freshly prepared sulfuric acid in methanol [5% (v/v)], 25  $\mu\text{L}$  of BHT solution [0.2% (w/v) butylated hydroxy toluene in methanol], 25  $\mu\text{g}$  of triheptadecanoin (as internal standard) and 300  $\mu\text{L}$  of toluene were stored at 4 °C, until all developing seeds from different DAP were harvested. Subsequent assays of direct methylation, extraction of fatty acid methyl esters, and analysis by gas chromatography was conducted as previous described.<sup>83</sup>

### Glucosinolate quantification

For glucosinolate analysis, three types of samples were prepared: 1) 10 seeds from individual, mature, intact siliques from fully senesced plants, 2) the non-seed silique tissues (valves, septa, replum) from the same individual siliques and 3) 5 mg of seeds, pooled from groups of four plants. Samples were collected in 85% (v/v) methanol containing *p*-hydroxybenzyl glucosinolate (pOHb, Extrasynthese Cat. No. 2511 S) internal standard and homogenized in a bead mill (Retsch, 3 mm bearing beads, 30s at 30 Hz). For analysis of glucosinolates as desulfo-glucosinolates, chromatography was performed on an Advance UHPLC system (Bruker). Separation was achieved on a Kinetex 1.7 $\mu$  XB-C18 column (100 x 2.1 mm, 1.7  $\mu\text{m}$ , 100 Å, Phenomenex). Formic acid [0.05% (v/v)] in water and acetonitrile [supplied with 0.05% (v/v) formic acid] were employed as mobile phases A and B respectively. The elution profile was: 0–0.5 min, 2% B; 0.5–1.2 min, 2–30% B; 1.2–2.0 min 30–100% B, 2.0–2.5 min 100% B, 2.5–2.6 min, 100–2% B and 2.6–4 min 2% B. The mobile phase flow rate was 400  $\mu\text{L min}^{-1}$ . The column temperature was maintained at 40°C. The liquid chromatography was coupled to an EVOQ Elite TripleQuad mass spectrometer (Bruker, Bremen, Germany) equipped with an electrospray ion source (ESI) operated in positive ionization mode. The instrument parameters were optimized by infusion experiments with pure standards. The ion spray voltage was maintained at +3500 V. Cone temperature was set to 300°C and cone gas to 20 psi. Heated probe temperature was set to 400°C and probe gas flow to 40 psi. Nebulizing gas was set to 60 psi and collision gas to 1.5 mTorr. Nitrogen was used as probe and nebulizing gas and argon as collision gas. Active exhaust was constantly on. Multiple reaction monitoring (MRM) was used to monitor analyte precursor ion  $\rightarrow$  product ion transitions. Detailed values for mass transitions can be found.<sup>95</sup> Both Q1 and Q3 quadrupoles were maintained at unit resolution. Bruker MS Workstation software (Version 8.2.1, Bruker) was used for data acquisition and processing. Linearity in ionization efficiencies was verified by analyzing dilution series. *p*-hydroxybenzyl glucosinolate was used as internal standard.

### Total lignin quantification

The lignin content was determined by the acetyl-bromide method, based on Barnes and Anderson's protocol with slight modifications.<sup>96</sup> The stems of plants grown to senescence were finely ground and 5–8 mg of each sample was weighed and placed in 12 mL glass screw-cap vials. The exact mass was recorded, and the five biological replicates were processed in technical triplicates. 1 mL of 25% (v/v) acetyl bromide in glacial acetic acid was added to each vial, with one empty vial serving as a blank. The vials were gently swirled and placed in a 70°C water bath. The vials were gently swirled three times during the 70 min incubation. The samples were then transferred to ice and 5 ml of glacial acetic acid was added to each sample. The vials were shaken thoroughly and left until any residues had precipitated at the bottom of the vials, a minimum of three hours up to overnight. Once settled, 30  $\mu\text{L}$  of each sample was transferred to a UV-transparent 96-well plate. To each well, 40  $\mu\text{L}$  of 2 M sodium hydroxide and 30  $\mu\text{L}$  of freshly prepared 0.5 M hydroxylamine hydrochloride were added. The samples were mixed thoroughly by pipetting, and absorbance was measured immediately at 280 nm.

### ChIP assay

ChIP assay was performed according to a protocol described previously<sup>97</sup> with modifications. In brief, 5 to 14 DAP siliques were ground to fine powder in liquid nitrogen and fixed with 1% (w/v) formaldehyde for 10 min under vacuum, followed by incubation at 4°C on a sample rotator for another 20 min. The crosslinker was quenched by adding glycine to the final concentration of 0.15 M. The chromatin was extracted by adding four volumes of nucleus fractionation buffer (15 mM PIPES pH 6.8, 250 mM Sucrose, 5 mM MgCl<sub>2</sub>, 60 mM KCl, 15 mM NaCl, 1 mM CaCl<sub>2</sub>, 0.9% (v/v) Triton X-100, 1 mM PMSF), followed by filtration through Miracloth and centrifuge. After preclearance with protein G magnetic beads (Thermo Fisher) and salmon sperm DNA, the sonicated chromatin was incubated overnight with or without anti-flag antibody (Proteintech). The purified protein-DNA complexes were recovered. DNA fragments were further purified by Monarch PCR & DNA cleanup kit (New England Biolabs). The primers used for ChIP-qPCR are provided in [Table S3](#).

### Recombinant protein production, purification, and EMSA

Protein expression vectors were transformed into *E. coli* [BL21 (DE3)] and selected on antibiotic-selective media. Protein induction, extraction and purification were conducted according to the protocols as previously described,<sup>98</sup> with slight modification. Cell cultures were induced at 22 °C for 2 h with 1 mM isopropyl-β-D-thiogalactoside (IPTG). EMSA was performed according to a protocol described previously,<sup>44</sup> with slight modification. The 5' end biotin-labeled (hot) and -unlabeled (cold) probes for the *proNST1* fragments containing (A/T)(G/C)TT sites (probe P6-1: 5'-TAGCAAACTATTTAAAAGTAGACGCCAAAAAAATTGAA-3'; probe P6-2: 5'-ACAAGAGAATAATAATCATTAAATAATTGACAAGTAAAAT-3'; probe P6-3: 5'-GGTTATATTTTAAATTTTCAAATAAATAATGAATACAAAT-3'; probe P6-4: 5'-TTGAATTTTAAATAATTAAGAAAAACAAAAAAGGTGTACA-3') were used. The standard binding reaction (20 μL) contained 10 mM Tris (pH 7.5), 50 mM KCl, 1 mM dithiothreitol, 2.5% (v/v) glycerol, 0.05% (v/v) IGEPAL CA-630, 5 mM MgCl<sub>2</sub>, 0.5 mM EDTA, 2.5 ng/mL poly(dI·dC), 50 fmol biotin-labeled probe, and 1 μg of purified GST-His-ZFP2. The reaction mixture was incubated at room temperature for 30 min. The DNA-protein complexes were separated on 10% (w/v) native polyacrylamide gels and subsequently transferred onto a nylon membrane. The band shifts were detected using chemiluminescent nucleic acid detection module (Thermo Scientific).

### QUANTIFICATION AND STATISTICAL ANALYSIS

Statistical significance was determined using one-way ANOVA or one-way ANOVA followed by Tukey-HSD test or Kruskal-Wallis test or Kruskal-Wallis test followed by Dunn's test or Welch's t-test, as described in the figure legends.